2(mod)

NASA CR112274

FEASIBILITY STUDY OF THE APPLICATION OF EXISTING TECHNIQUES TO REMOTELY MONITOR HYDROCHLORIC ACID IN THE ATMOSPHERE

SUBMITTED TO

NASA LANGLEY RESEARCH CENTRE

HAMPTON, VIRGINIA

SUBMITTED BY

BARRINGER RESEARCH LIMITED
304 CARLINGVIEW DRIVE
REXDALE, ONTARIO, CANADA

TR73-226 A

PREPARED BY: H. Zwick

V. Ward

L. Beaudette

APPROVED BY J. H. Davies
General Manager, R & I Division

APRIL 1973

CONTENTS

SUMMARY

This report was prepared under NASA contract NASI-11923. The scope of the work includes a critical evaluation of existing optical remote sensors for the specific problem of HCl vapour detection in the plumes of solid propellant rockets.

The work performed includes, a selection of the P branch of the fundamental vibration-rotation band as the most promising spectral feature to sense, a computation of transmittance for HCl vapour, an estimation of interferent spectra, the application of these spectra to computer modelled remote sensors, and a trade-off study for instrument recommendation.

Section 1

INTRODUCTION

Solid propellant rockets are expected to inject a variety of gases into the atmosphere. These vapours include such potentially dangerous gases as CO, Nitrogen oxides and HCl. The total amounts of these materials injected into the atmosphere by launches of different vehicles has been computed and is shown in Figure 1. This figure is taken from NASA draft report EIS-AA-724988D. (1972). The quantities in NASA report EIS-AA-72-4939F agree reasonably well with those given in Figure 1.

These gases are ejected from the rocket engine at velocities in the region of 8000 feet/second and at a stagnation temperature of 5,500^{o}F. (NASA report N72-22790). This hot cloud rises rather quickly due to its bouyancy, and through mixing and adiabatic expansion will reach an altitude and temperature where it is in equilibrium with its surroundings. This relaxation process should occur rather quickly. Some experimental measurements by Forbes et al (NASA report CR-2049), who flew an aircraft through the exhaust clouds of rockets, observed that the cloud temperature approached that of its surroundings within a few minutes of launch. Further, Block Engineering (USAF, Giffiths AFB report SIVS/R-23) observed that the cloud temperature dropped so quickly that it was difficult in their experiment to record emission from the cloud after the first minute.

Following this relaxation, where the cloud comes to an equilibrium bouyancy with its surroundings, the usual diffusive and convective transport mechanisms will begin to disperse the cloud. The dispersion pattern from such clouds has been computed (NASA report EIS-AA-72-4988D) and a reproduction of the estimated HCl concentration as a function of downwind distance is given in Figure 2 for the case of a low level Titan 111C abort.

The ultimate fate of HCl vapour is not known. However, because HCl is a reactive gas, extremely hygroscopic, and highly soluble in water it is very probable that HCl will be removed by the atmospheric aerosol and by soil or water at the earth's surface. Remote sensing instrumentation could be used to evaluate such possible sinks, in addition to determining the

QUANTITIES OF POTENTIAL POLLUTANTS EMITTED INTO SELECTED ATMOSPHERIC LAYERS

Note: To convert to pounds, multiply kilograms by 2.20

Atmospheric Layer Altitude Range	Nocturnal Inversion 0-500 m			Subsidence Inversion 0-1500 m			Troposphere 0.5-20 km			Stratosphere 20-67 km					Mesosphere-Thermosphere Above 67 km				
	Emission, kg																		
Vehicle	HCl	CO	NO*	HCl	CO	NO*	HCl	CO	NO*	HCl	CO	NO*	CO_2	H_2O	HCl	CO	NO*	CO_2	H_2O
Scout	60	110	nil	180	310	0.5	2,290	1,240	6.4	760	970	2.3	100	340	450	830	1.4	64	198
Delta(3C)	690	2,600	1.8	1,130	4,120	3.2	1,710	10,790	4.5	0	14,400	0	10,700	9,300	0	3,360	70	3,970	2,990
Delta(6C)	830	2,500	2.3	1,840	4,260	5.0	3,920	11,320	11	0	14,900	0	11,100	9,700	0	4,930	70	3,650	3,270
Delta(9C)	1,100	3,020	3.2	1,750	4,550	4.5	5,630	13,740	15	410	13,350	0.9	9,600	8,400	0	5,830	70	4,340	3,800
Atlas/Centaur	0	6,310	0	0	10,030	0	0	24,310	0	0	17,500	0	13,100	11,400	0	4,540	0	3,380	15,760
TIIIE/Centaur**	9,800	17,510	30	14,920	26,540	41	47,170	83,000	126	24,040	43,320	750	19,700	18,800	0	3,060	1,530	20,400	47,450

* The NO formed from N_2 impurity in the stages using liquid oxygen (Atlas, Thor, Centaur) is not included. The concentration of NO in the exhaust of such stages has been estimated at 3 ppm for an N_2 impurity level of 600 ppm.[13] The resulting NO emissions are negligible.

** The Titan IIIC is equivalent to the TIIIE/Centaur except for changes in the emissions above 67 km. These changes are not significant in terms of upper atmosphere effects.

FIGURE 1

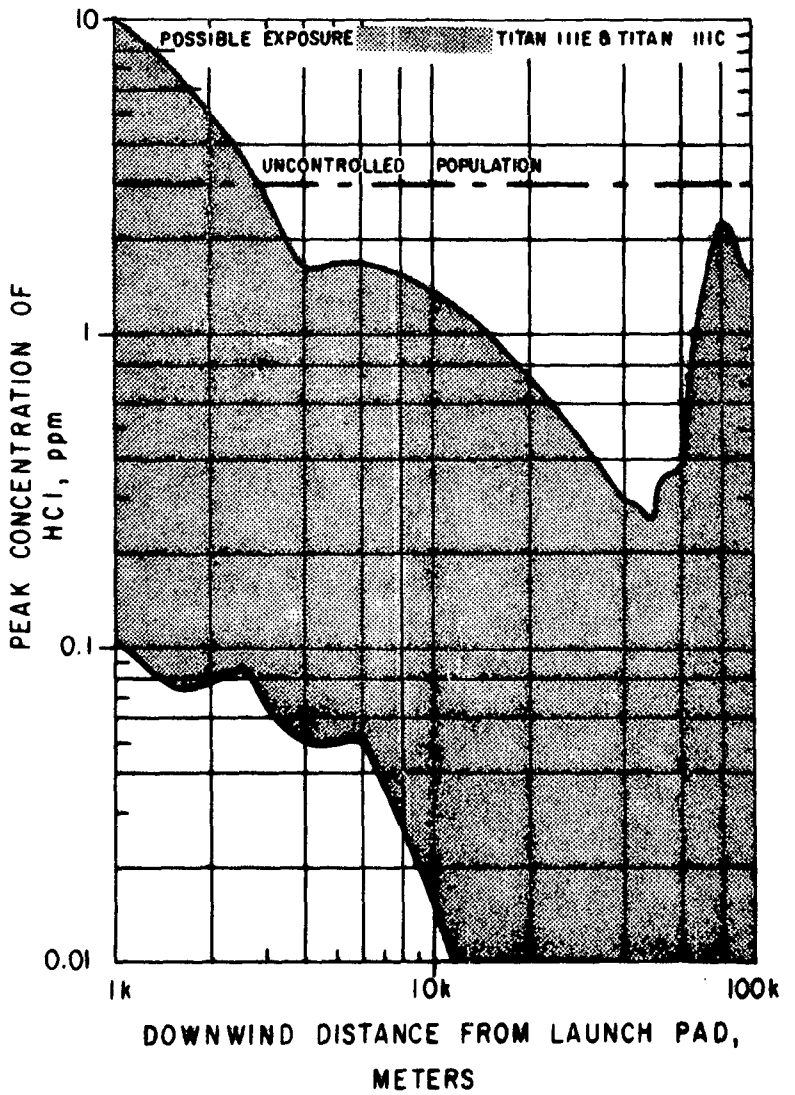

FIGURE 2. ESTIMATED PEAK HCl CONCENTRATIONS DOWNWIND OF ON-PAD ABORTS. BANDS FOR EACH VEHICLE INCLUDE RESULTS FROM ANALYSIS FOR THREE ATMOSPHERIC STABILITY CRITERIA AND THREE INVERSION HEIGHT.

degree of pollution due to the launch of these vehicles.

HCl may be detected by a variety of methods including gas chromatography, chemical techniques and perhaps tuneable laser systems. Remote sensors which are capable of detecting the total burden of vapour in the sensor field of view without the need of active sources are however very attractive for mapping plumes, where large area coverage in a short time is required.

Barringer Research Limited has developed a variety of optical correlation sensors which are capable of rapid and specific detection of chosen gases. The first such instrument developed was the correlation spectrometer (COSPEC) described initially by Barringer and Schock (1966) and subsequently in several reports and also in a recent paper by G. S. Newcomb and M. M. Millan (1970). This instrument is being sold commercially primarily to users interested in total SO_2/NO_2 burdens. The correlation interferometer has been under development for several years, and has also recently been described by Dick and Levy (1970), and by Grenda et al (1971).

The final Barringer correlation device is a gas cell non-dispersive analyzer, with recently devised compensation techniques which cause the instrument to be insensitive to operating environmental conditions. This instrument has not been described in the open literature and a breadboard version is being fabricated at Barringer Research at the time of writing.

In addition to this instrument there are several additional manufacturers of interferometers including Block Engineering and others. These are reviewed by Bell (1972). Furthermore, General Dynamics have over the past several years developed a non-dispersive infrared gas cell analyzer called a Gas Filter Correlation sensor which has been described by Ludwig et al (1968, 1969) and Bartles et al (1971).

The scope of the present work is to evaluate the feasibility of applying these optical correlation remote sensing devices to the problem of detection of HCl vapour in the plume of solid propellant rocket exhausts.

Section 2

SPECTRA AND ATMOSPHERIC EFFECTS

2.0 THE HCl SPECTRUM

The HCl spectrum contains electronic transitions which occur in the 1300Å region. These are too far into the ultraviolet region of the spectrum to be useful for remote sensing. This is because of strong absorption due to O_2 and other atmospheric constituents which remove the solar energy in the higher atmosphere.

The microwave spectral region contains the pure rotational spectrum of HCl, however at the pressure of the atmosphere near the earth's surface it is unlikely that specific detection is possible here.

There remains the vibrational-rotational spectral structure which for the fundamental transition occurs at about 3.5 microns. The HCl vibrational-rotational structure is shown in Figure 3. It is this spectral region which has been selected as the most promising for the remote detection of HCl in the atmosphere.

The HCl transmittance spectra were computed by a local university using a radiative transport computer programme (Cann and Nicholls, 1972).

The HCl transmittance spectrum was computed for a 295°K isothermal atmosphere, for a 2 kilometer path of HCl at concentrations of 0.5 parts per billion (ppb), 5 ppb and 50 ppb so that the integrated HCl burdens were 1 ppm-m, 10 ppm-m, and 100 ppm-m. These amounts are well below the anticipated initial burden of more than 1000 ppm-m based on measurements made by Block Engineering (USAF, Griffiths AFB report SIVS/R-23).

A sample of the HCl computed transmittance (1 ppm-m) is shown in Figure 4.

The transmittance due to these burdens of HCl were used to evaluate the

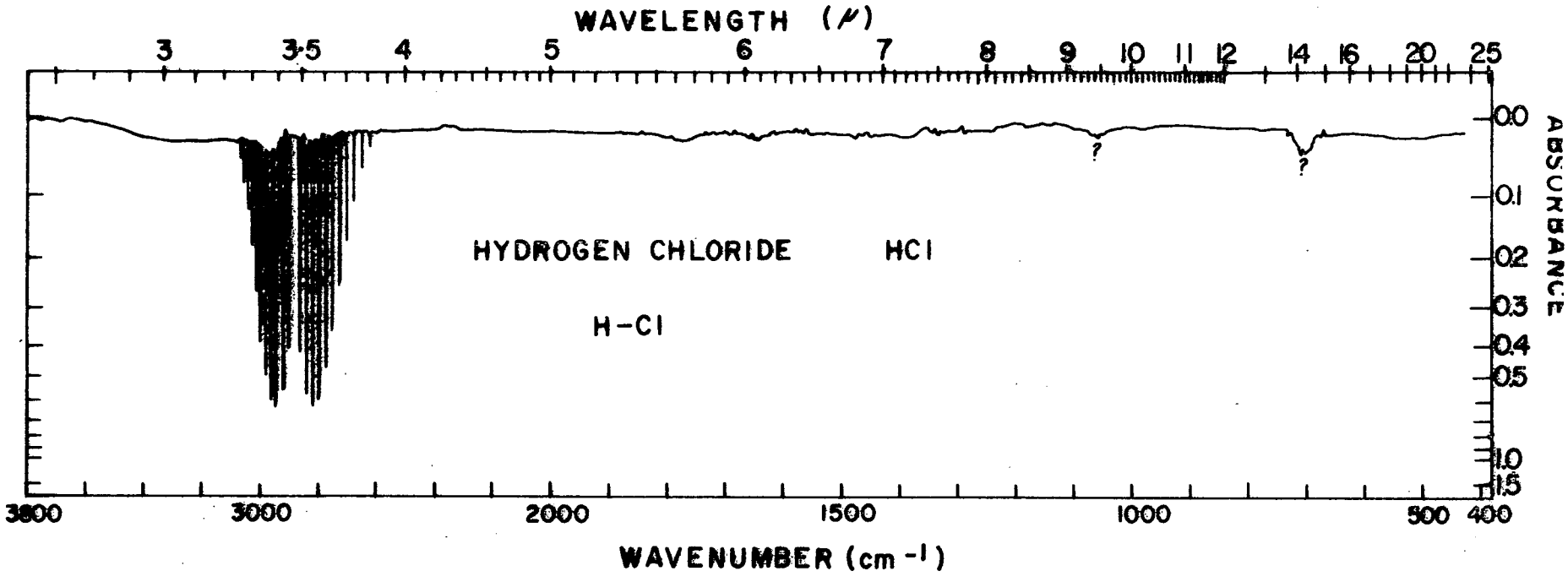

FIGURE 3. HCl ABSORPTION SPECTRUM

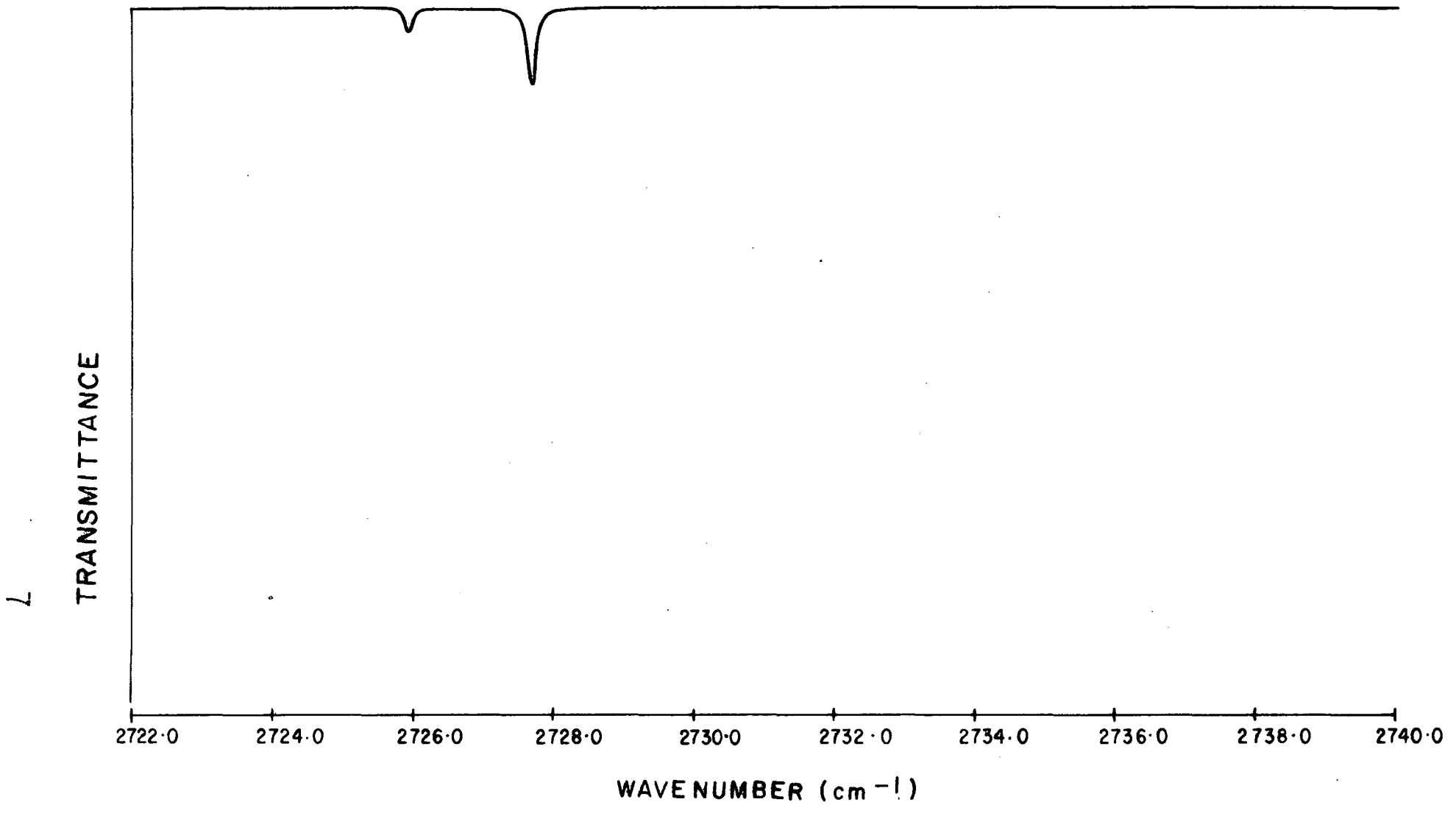

FIGURE 4. HCL COMPUTED TRANSMITTANCE FOR 0·5 ppb OVER A 2 km PATH OF 295°K ISOTHERMAL ATMOSPHERE

change in spectral radiance at the sensor, and this coupled with the transfer function of the instrument enabled the evaluation of instrument sensitivity.

2.1 SPECTRAL INTERFERENTS

Two sources of spectral interferents are the natural species normally found in the atmosphere, and those species introduced by the solid propellant rockets at the same time as the HCl target vapour. An indication of the naturally occuring spectral interferents was estimated from Migeottes Atlas. From this atlas it is evident that the R branch of the HCl band is rather badly interferred with by methane, and the P branch, although somewhat "cleaner", has some N_2O interference and some water absorption lines are also present. In addition the atmospheric aerosol and the Rayleigh wings of distant bands tend to cause a general decrease in transmittance with increasing zenith distance. The aerosol extinction coefficients given by McClatchey et al (1972) show that horizontal geometry will result in a rather low transmittance. The result of this is a rather "warm" black body radiator against which the emission of HCl will be difficult to detect.

The interferents produced by the launch vehicle will most probably include aerosol material composed primarily of Al_2O_3 in the 1 to 40 micron diameter region. In addition, surface dust will be raised by the high velocity effluent, and finally, it is possible that minor amounts of N_2O are produced. It is clearly a requirement of a successful HCl detector that it be able to discriminate against these interferents.

Another possible class of interferent vapours are the hydrocarbon CH strech band features near 3.5 microns. The degree to which these present possible interferent responses are difficult to predict unless each species can be individually assessed. Again experimentation would appear the most effective approach.

So as to incorporate spectral interferents in a somewhat more realistic fashion, the atmospheric transmittances TR_ν^i were obtained from Migeottes atlas, and this was used to estimate the interferent spectrum. This was chosen over the rather unattractive alternative of incorporating all of the

possible interferent gases (CH_4, N_2O, H_2O, etc) and aerosol effects. To evaluate the effect of changing amounts of interferents in the atmosphere, the transmittance spectrum of Migeotte was modified. The simple procedure of taking the square and the cube roots of TR_ν^i were chosen as the interferent changes. These changes were presented to each sensor model to evaluate the change in response caused by this interference.

An example of a section of Migeottes atlas transmittance is given in Figure 5.

2.2 ATMOSPHERIC PHYSICS OF REMOTE SENSING

2.2.1 Measurements Made in the Downward Looking Mode

At wavelengths below about 3μ the solar radiance reflected from the earth's surface is greater than the thermal emission from the surface. The wavelength at which the reflected radiance equals the emitted radiance depends on the sun zenith angle, cloud cover, the surface reflectivity and emissivity, and on the surface temperature. In general however, this cross-over region is about 3 microns. The P branch centered at about 3.6μ would normally be expected to have about 10 times more radiance emitted from the earth than the reflected solar radiance (Wolfe, 1965). For early morning, late evening, or night time launches, the solar contribution can be neglected, and this should be the case even during daytime launches. Certainly for detection requiring no more than 10% accuracy it should be possible to neglect the solar radiance term.

Appendix A suggests that under certain assumed conditions the spectral radiance $N_\nu(S)$ at the instrument sensor can be expressed approximately as

$$N_\nu(S) = \varepsilon_E B_\nu(T_E) Tr_\nu(S) + (1 - Tr_\nu(S))B_\nu(T_A) \qquad (1)$$

where ε is emissivity, B_ν the black body radiance at temperature T and $T_{r_\nu}(S)$ is the spectral transmittance through the atmosphere to S.

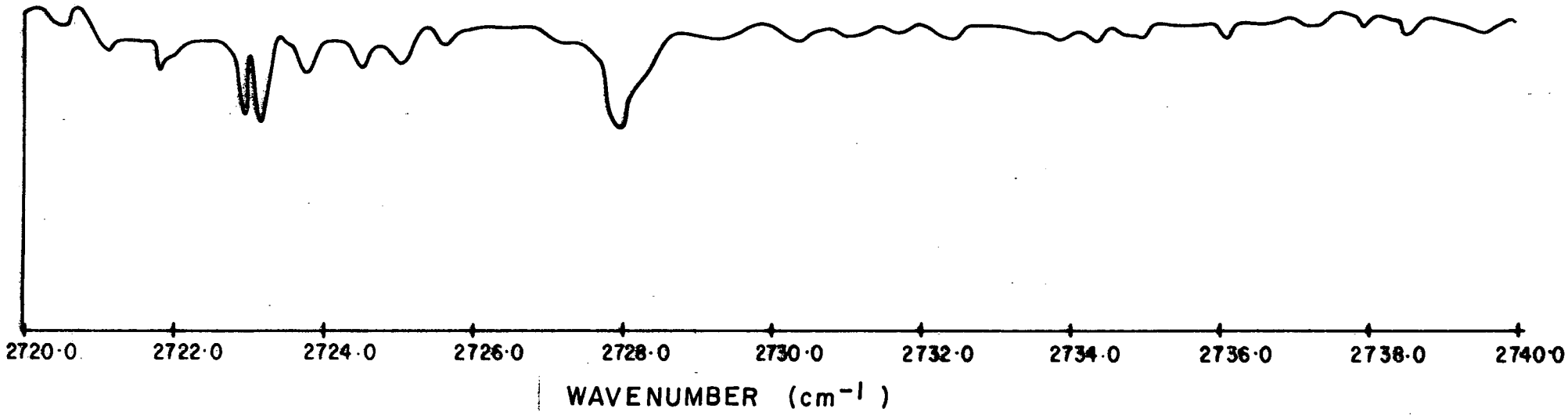

ATMOSPHERIC TRANSMITTANCE FROM MIGEOTTES ATLAS

FIGURE 5

The subscripts E and A refer to the earth's surface and the atmosphere respectively. It is evident that if $\varepsilon_E B_\nu(T_E) = B_\nu(T_A)$ one may write,

$$N_\nu(S) = B_\nu(T_A)$$

which shows that the spectral radiance is independent of the atmospheric transmittance and gas detection is impossible with these assumed conditions.

Figure 6 shows that typically each morning and evening there is a time when the earth's surface temperature equals the air temperature. If the surface emissivity is approximately 1, there will be times during which normal downward detection of atmospheric vapour is not possible. However, measurements even at these times may be possible if one can harness naturally occurring variations in the albedo. This so called "ground chopping" technique has been described (Zwick and Millan, 1971).

Ground chopping is a technique which relies on the spatial variations in surface radiance (caused by emissivity and temperature variations). If the sensor "footprint" on the surface is small there will be a time varying radiance from the surface as the footprint spatially scans the non-homogeneous surface. If the sensor electronics is band limited so that only the time varying spectral radiance, n_ν, is accepted (AC coupled) then the spectral radiance at the sensor becomes

$$n_\nu(S) = n_\nu(o)\ Tr_\nu(S) \qquad (2)$$

The emission from the atmosphere will only vary slowly in time as the spatial extent of the pollution cloud is large with respect to the footprint size. Such slow variations may be rejected by the electronics. Only rapid atmospheric temperature variations could result in a radiance fluctuation which could be passed through the filter, but these are expected to be small.

Ground chopping has not been demonstrated in the infrared but it seems worth consideration and testing for many terrain types.

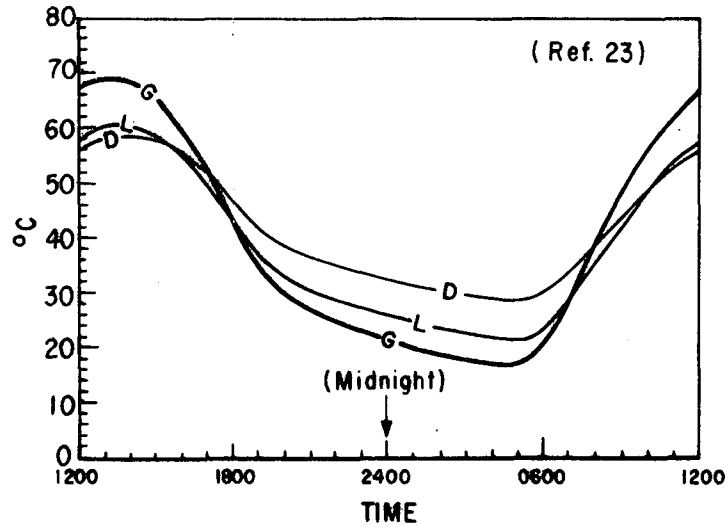

DIURNAL VARIATIONS IN THE SURFACE TEMPERATURES OF (L) LIMESTONE, (D) DOLOMITE AND (G) GRANITE IN MIDSUMMER

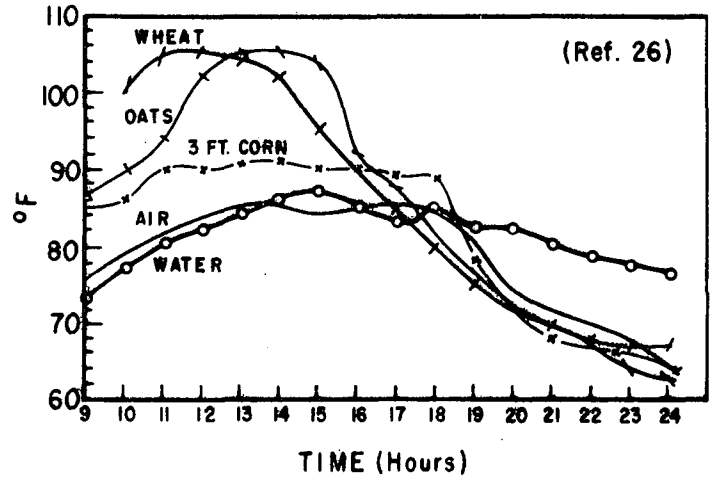

TEMPERATURE VARIATIONS OF CROPS

FIGURE 6.

Downward looking sensors can however be used for HCl detection when the atmosphere and the earth's surface differ in radiance, as is normally expected near mid-day or near mid-night.

2.2.2 Measurements in the Upward Looking Mode

An upward looking system has the advantage that the rather small radiance of space can be used as a background against which the emission of HCl at atmospheric temperatures can be sensed. The other upward looking geometry is to use the sun as a source, however for plume mapping the additional complexity of maintaining solar sighting is undesirable. For the case of an upward looking sensor not looking at the sun, the spectral radiance can then be written as

$$N_\nu(S) = (1 - TR_\nu(S))\ B_\nu(T_A) \tag{3}$$

If the transmittance is expressed in terms of the target vapour transmittance times the interference vapour plus the aerosol transmittance, one obtaines

$$N_\nu(s) = (1 - TR_\nu^i(S)\ TR_\nu^g(S))\ B_\nu(T_A) \tag{4}$$

In the upward looking mode the interference transmittance is that integrated along the line of sight of the sensor through the whole atmosphere. Obviously for angles approaching the horizontal, TR_ν^i becomes small.

A rather crude extrapolation of Etermans (1970) data to 3.6 microns to the case of a visual range of 10 km suggests an extinction optical thickness of about 0.2. If one makes the crude assumptions that the atmosphere is isothermal up to 1 km, and so cold above that the radiance from greater altitudes may be neglected, then the effective extinction thickness is that between 0 and 1 km, or about 0.1. Further, according to Hodges (1972), about 10% of the extinction at 3.6μ is due to absorption (and thus presumably can be re-emitted), so that the effective optical thickness due to this 1 km isothermal absorber would be about 0.01.

Although this thickness should increase with angle, according to sec θ approximately, rather large zenith angles should be possible before detection is severely limited. These calculations are very crude, and allowance is not made for the aerosol generated by the launch vehicle. These effects will require experimental evaluation, but the indications are that this operational mode should also be feasible provided the sensor has sufficient sensitivity.

Section 3

OPTICAL CORRELATION REMOTE SENSORS

3.1 INTRODUCTION

The theory and operation of some remote sensors are outlined in this section. Since a comparative study is to be made, several features have been chosen as indicative of sensor capability. These features include sensitivity, specificity, observation and integration time, size-weight-and-complexity, and cost. As these are features common to each instrument, some discussion of these will preceed the actual instrument discussion.

3.1.1 Sensor Sensitivity

The sensor whose sensitivity to HCl is greatest is the most desirable. Sensitivity to an integrated burden of approximately 30 ppm x 100 meters is about the upper limit expected in the ground cloud, and to be useful the sensor should be capable of sensing HCl burden several orders of magnitude lower than this.

The instrument sensitivity can be specified in terms of the power change at the detector caused by the presence of the HCl vapour.

The power P, reaching the detector when no HCl vapour is in the atmosphere is

$$P = \int N_{\nu}^{i}(S)\ \tau A\Omega\ d\nu \qquad (5)$$

where $N_{\nu}^{i}(s)$ is the spectral radiance at the sensor collector when no HCl is in the atmosphere

A is the collector area

Ω is the solid angle of acceptance of the collector

τ is the spectral efficiency of the sensor through to the detector and for convenience is written as the product of the average transmittance τ_o times the relative spectral transmittance τ_ν.

$$\tau = \tau_o \tau_\nu$$

The function τ_ν is the relative instrumental transfer function.

The change in power, S, at the detector caused by the presence of the HCl vapour is

$$S = \int_\nu (N_\nu^i(S) - N_\nu^g(S))\ \tau_\nu\ A\Omega\tau_o\ d\nu \qquad (6)$$

Where $N_\nu^g(S)$ is the spectral radiance at the sensor collector when HCl vapour is present.

If one assumes a detector noise limited device, as may be expected for an infrared sensor system, the noise power level, NEP is given by

$$NEP = \frac{(A_d \Delta f)^{1/2}}{D^*} \qquad (7)$$

Where A_d is the detector area

Δf is the effective bandwidth which is related to the integration time T_m by $T_m = 1/(2\pi\Delta f)$

and D^* is the figure of merit of the detector. Hence the signal-to-noise may be written as

$$S/N = \left[\int_\nu (N_\nu^i(S) - N_\nu^g(S))\ \tau_\nu d\nu\right]\ A\Omega\tau_o D^*/(A_d\Delta f)^{1/2} \qquad (8)$$

For the sensor types to be considered, the variables are A, Ω, τ_o, and τ_ν and A_d. The same detector type will be assumed for each instrument and the integration time will be assumed equal in each case.

3.1.2 Sensor Specificity

The specificity is defined as the degree to which the sensor response is insensitive to interferent species. In the case of a classical single entrance slit, single exit slit spectrometer the specificity could be rather simply related to the instrument resolution. The higher the resolution the better the

rejection of interferent species, up until instrumental bandwidth is narrower than the target spectral feature. This same concept is true of correlation instruments. However, with greater specificity goes a lesser sensitivity. In the case just cited, the narrower spectrometer slits have less radiant throughput or étendue. In fact the resolution-étendue product is a constant for grating spectrometers (James and Steinberg, 1969).

In the case of optical correlation instrumentation the effect of reducing resolution so as to increase sensitivity results in a loss of interferent rejection which is not so obvious to evaluate as with conventional devices. It is possible by judicious choosing to accentuate certain target spectral features which have few interferents, and to reduce the influence of those regions which have serious interferents.

It is because of this complex spectral trade-off that computer programmes were devised to simulate the response of each sensor and to evaluate the ability of each to reject a simulated spectral change in atmospheric radiance.

3.1.3 Observation and Integration Time

Commercial instrumentation is usually designed so as to enable reconstruction of the spectral radiance of the scene being viewed. Hence it is usual for spectrometers and interferometers to require of the order of seconds to complete one spectral scan (interferogram in the case of interferometers). Bell (1972) gives a review of commercial interferometers available in about 1970.

With correlation instrumentation however the situation is quite different. Because the instruments are by nature multiplexed (observe all desired spectral features simultaneously) it is only necessary to oscillate between two pre-chosen multiplex positions or regions in order to execute a measurement. This oscillation can be performed in about one second with correlation interferometer sensors, about 10 milliseconds with some correlation spectrometers, and several thousandths of a second for some correlation gas cell analyzers.

It is this possibility of very fast observational measurement which makes the optical correlation instruments ideal for airborne sensing, or for studying the dynamics of flow systems such as cloud dispersion where fast large area coverage is required.

3.1.4 Size, Weight and Complexity

Other trade-off parameters to consider in evaluating an instrument for a specific task include size, weight, complexity and ruggedness. The sensor best suited for plume dynamic coverage must be rugged and portable. Again optical correlation sensors score heavily in these categories.

3.1.5 Cost

Obviously the most cost effective instrument is that one which performs the desired measurement at the least cost. A cost evaluation for each sensor will be given in a following section.

3.2 CORRELATION SPECTROMETER

3.2.1 Introduction

Several optical correlation sensors have been developed which offer the possibility of sensitive, rapid remote monitoring of integrated gas burdens along the line of sight of the sensor. Correlation spectroscopy instrumentation, using grating spectrometers have been discussed by Barringer and Schock (1966), Ludwig et al (1968), Williams and Kolitz (1968), Millan et al (1969), Davies (1970), Newcomb and Millan (1970), Millan (1971), and Moffat et al (1971). The closely related technique of Hadamard Spectroscopy has been discussed by Ibbet et al (1968), Decker and Harivet (1968), Nelson and Fredman (1970). The use of multiple entrance slits for added throughput or etendue, has resulted in a coming together of classical spectroscopy and Hadamard Spectroscopy.

The name of correlation spectroscopy arises from the fact that the observable chosen as output is the variation of the correlation function between a mask, or array of exit slits, situated in the exit plane of a spectrometer, and the dispersed power spectrum, produced in the spectrometer. The correlation function between the dispersed power spectrum of the incoming light and the array of slits is the power in watts passing through the mask, from the dispersed power spectrum to a photo-sensitive device situated behind the mask. The correlating function may be of the matched filter type to match the absorption spectrum of the absorbing target gas, or the filter may be optimized to give a minimum rms response due to anticipated interferents. A correlation spectrometer is designed to detect the quantity of a specific gas present in the line of sight by displaying the dispersed spectrum of incoming radiation at the exit mask. The mask structure allows alignment to specific absorption bands of the gas under investigation.

Modulation is produced either by oscillating the spectral position relative to the correlation mask, or alternatively by cyclically moving the mask position as seen by the detector. The modulation is detected by a detector and electronically processed to provide an output proportional to the concentration pathlength product. The optical layout of one such device is shown schematically in Figure 7.

3.2.2 Operational Description

The dispersive correlation spectrometer consists of fore-optics, a modulator, grating spectrum disperser, exit mask, detector and associated electronics. The modulator may consist of a pair of refractor plates mounted in the end of one of the arms of a tuning fork, which is driven at its resonant frequency (normally in the 100 - 1000 Hz range). The movement of the plates causes the light beam to "jump" cyclically between two predetermined positions, (1) and (2). The distance between the positions is determined by the refractor plates' thickness, angle between plates and wavelength of radiation. (In another configuration the masks are mounted on a rotatngg disc which alternately passes a pre-chosen set of spectral wavelengths to the detector).

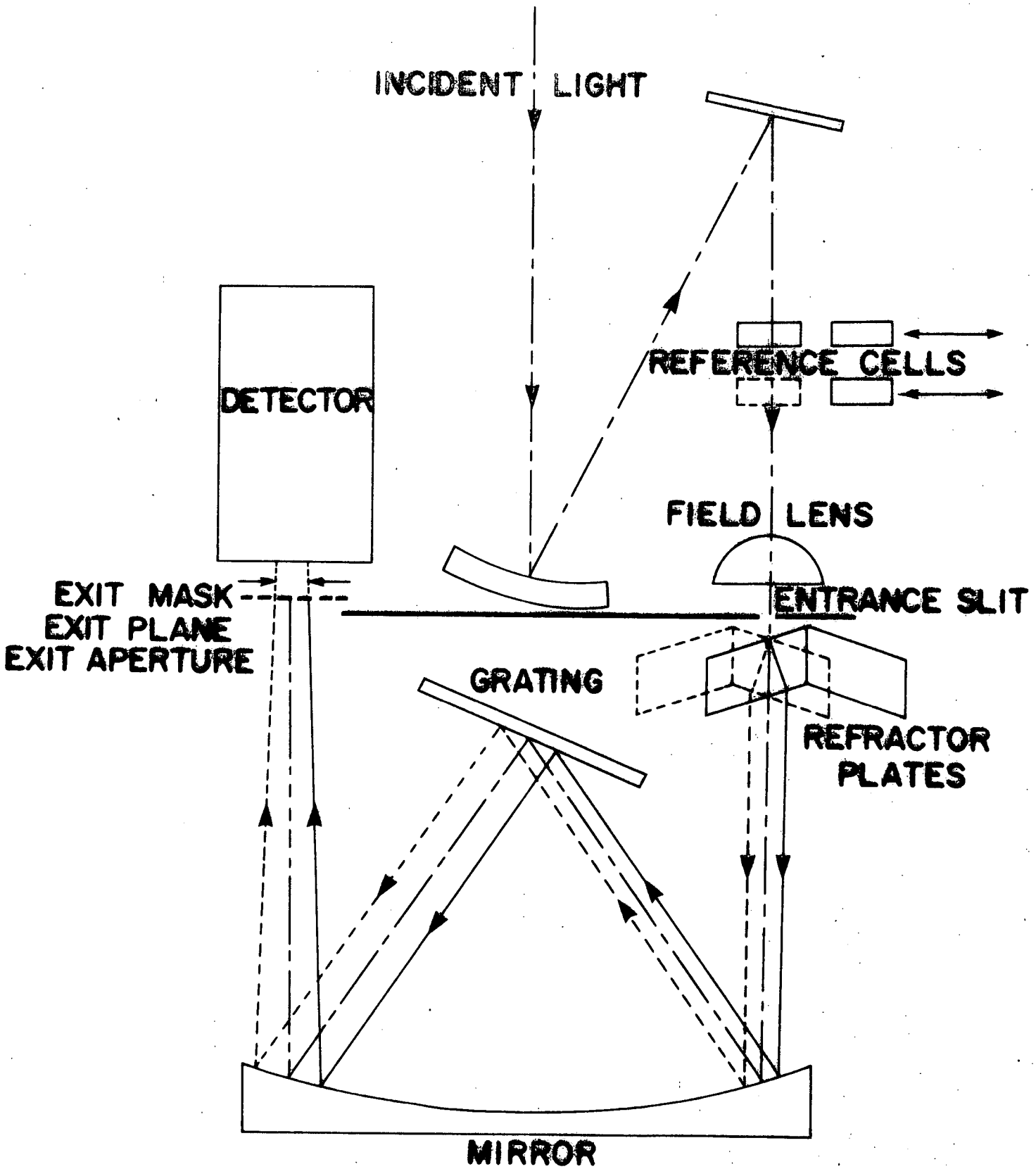

FIGURE 7.

SCHEMATIC LAYOUT OF A CORRELATION SPECTROMETER

The dispersed spectrum in the exit plane of the polychromator is a multi-wavelength image of the entrance slit. The position of any predetermined wavelength with respect to a set of fixed axis in the exit plane is governed by the grating angular position.

The mask or array of exit slits is situated in the exit plane in front of a detector. The response of the detector-preamps is a variable quantity. In order to control the amount of current from the detector under varying light conditions, an automatic gain control (AGC) is normally used, which together with the synchronous detector perform the following functions:

(a) One of the positions of the spectrum with respect to the exit mask and with incident power P_1 is selected to control the AGC.

(b) The AGC loop is phase-locked to this position and a fixed signal S_1 is selected according to the expected use of the instrument. The gain is automatically adjusted so that the response to mask position 1 is always S_1.

(c) The second position of the spectrum with respect to the mask with incident power P_2 generates a detector signal S_2.

(d) The process is repeated for each oscillation of the fork.

(e) A reference signal is obtained directly from the fork oscillation and a gate waveform is derived to be used in the synchronous detector.

(f) S_2 will vary with respect to S_1 as a function of the characteristics of the dispersed spectrum.

(g) The product detector waveform is passed through an integrator and a signal output is presented to the recording device.

The difference signal is given by

$$S = (S_1 - S_2)\, d$$

where S_1 (fixed) $\alpha\ P_1\ G_j\ G \alpha \dfrac{S_1}{P_1}$

and $S_2\ \alpha P_2\ G\ \alpha S_1 \dfrac{P_2}{P_1}$

The signal current then becomes:

$$S = dS_1 \left\{ 1 - \frac{P_2}{P_1} \right\} \tag{9}$$

where d is the duty cycle of the gate waveform and will be included into τ_o the optical efficiency in the remainder of this report.

The AGC circuit is provided for two main reasons:

(a) to provide automatic normalization between output current in mask positions (1) and (2), thus compensating for multiplicative changes in radiance level.

(b) to maintain constant the output current of the detector from one of the (mask-spectrum) positions thus providing a normalizing reference and easing the power supply demand on the detector.

The AGC then provides a feedback loop which adjusts the effective gain.

The étendue achievable with a dispersive spectrometer is limited by the entrance slit width in the direction of dispersion, due to whatever resolution is required. Slit heights can, on the other hand, be made fairly large. Efficiency in transferring gas modulated radiation to the detector is reasonably good. Many of the optical surfaces may be anti-reflection coated; the main loss is in the grating efficiency. The use of a mask in the plane of the spectrum allows the best possible modulation to be obtained, within the limits of resolution and the requirement for avoiding regions subject to interferences.

Attenuation of interferent takes the form of avoiding affected spectral regions where possible, and balancing them against each other where not.

Hence the device transfer function τ_ν is

$$\tau_{\nu 1} = F_\nu M_{\nu 1} \text{ and } \tau_{\nu 2} = F_\nu M_{\nu 2}.$$

The device response S_1 and S_2 when only interferents are present are

$$S_1 = G.\ A.\Omega.\tau_o \left[\int_\nu N_\nu^i\ (S)\ .\ \tau_{\nu_1}\ d\nu\right]$$

$$S_2 = G.\ A.\Omega.\tau_o \left[\int_\nu N_\nu^i\ (S)\ .\ \tau_{\nu 2}\ d\nu\right] \qquad (10$$

F_ν is the interference filter function which isolates the P branch of HCl, $M_{\nu 1}$ and $M_{\nu 2}$ are the two mask functions obtained from the convolution of the entrance slit and the exit slits.

The response $S^i = S_1^i - S_2^i$ will be an offset response; constant to the extent the instrument is insensitive to interferents.

The downward looking HCl response (from equation 1) can be written as $S_d = S^g - S^i$

$$S_d = GA\Omega\tau_o \left[\int_{\nu_1} M_\nu F_\nu \left\{\varepsilon_E B_\nu(T_E)\ Tr_\nu^i\ (S)\ TR_\nu^g\ (S) + B_\nu(T_A)\ (1 - Tr_\nu^i(S)\ Tr_\nu^g\ (S))\right\}\ d\nu\right.$$

$$\left. - \int_{\nu 2} M_\nu F_\nu \left\{\varepsilon_E\ B_\nu\ (T_E)\ Tr_\nu^i\ (S)\ Tr_\nu^g\ (S) + B_\nu(T_A)\ (1 - Tr_\nu^i(S) \times Tr_\nu^g(S)\ d\nu\right]\right.$$

$$- S^i$$

This reduces to

$$S^d = GA\Omega\tau_o \left[\int_{\nu_1} M_\nu F_\nu X_\nu^d \, d\nu - \int_{\nu_2} M_\nu F_\nu X_\nu^d \, d\nu \right] \tag{11}$$

where $X_\nu^d = \varepsilon_E B_\nu(T_E) \; Tr_\nu^i(S) \; (1 - Tr_\nu^g(S)) - B_\nu(T_A) Tr_\nu^i(S) \; (1 - Tr_\nu^g(S))$

When ground chopping is employed the above equation has a new value of X_ν given by

$$X_\nu^{gc} = c \; Tr_\nu^i(S)(1 - Tr_\nu^g(S)) \tag{12}$$

where C is the a.c. component of $\varepsilon_E B_\nu(T_E)$. For the computation C was chosen to be 10% of $\varepsilon_E B_\nu(T_E)$.

In the upward looking mode the signal response due to HCl vapour is obtained from equation 11, but where X_ν is (using equation 4)

$$X_\nu^u = B_\nu(T_A) \; Tr_\nu^i(S) \; (1 - Tr_\nu^g(S)) \tag{13}$$

3.2.3 Correlation Spectrometer Parameters for HCl Detection

The masks were chosen so as to transmit six H^1Cl^{37} P branch lines (P_2 through P_7), and the spectral width of the entrance and exit mask were chosen to be approximately 2 cm^{-1} wide (25Å). Mask 1 was placed so as to centre the transmission function on the line location, and mask 2 was chosen to be centered 3.5 cm^{-1} toward larger wavenumbers.

Other instrumentation parameters were

$$A\Omega = 1.4 \times 10^{-3} \text{ cm}^2\text{Sr}$$
$$\tau_o = 0.13$$
$$A_d = .16 \text{ cm}^2$$
$$D^* = 10^{11} \text{ cm Hz}^{1/2} \text{ W}^{-1}$$
$$\Delta f = 1 \text{ Hz}$$

The computer programs are discussed briefly in Appendix D. The results of this modelling are given in the next section.

3.3 CORRELATION INTERFEROMETER

3.3.1 Introduction

An interferometer transfers to the detector not the radiation at a given wavelength as does a dispersive spectrometer, but rather the interferogram (fourier transform) of the radiation. The relationship between the two is outlined in Appendix B. The output takes the form of cyclic variation of the amount of radiation transmitted, going through approximately one cycle or "fringe" for each wavelength change in interferometer delay. Ordinarly interferometry has advantages over dispersive spectrometry in two respects.

The radiance throughput or étendue, (the amount of available radiation which the device can accept) is usually greater for an interferometer than for a dispersive spectrometer. The interferometer is also completely multiplexed compared to the correlation spectrometer which often uses only the main spectral features. A Hadamard spectrometer in principle has the multiplex and étendue advantages of ordinary interferometers. Block Engineering have on the market a family of ordinary Michelson interferometers.

There are however certain forms of interferometers which enjoy additional advantages over ordinary Michelson or Fabry-Perot interferometer designs. Connes (1958) has devised a spherical Fabry-Perot design which at high resolution has an étendue advantage. Hansen (1941) and subsequently many others have shown that a Michelson interferometer may be field widened so as to have an additional radiance throughput advantage over ordinary Michelson interferomters. Reviews of this principle may be found in Steel (1967), James and Steinberg (1969).

Simply stated, field widening occurs when there is an uncompensated thickness of refractive material in one arm of the interferometer. The field widened condition occurs when the image position of one mirror is coincident with the second mirror position but the additional refractive material in one of the arms results in a non-zero delay. The interferometer depth-of-focus for a plane parallel slab of refractive material in one arm has been computed by Hilliard and Shepherd (1964) and derived by Zwick and Shepherd (1971). Barringer Research Limited has developed a correlation interferometer (Grenda et al, 1971) which scans a small delay region centred about the field-widened position. In this case the scanning is achieved by rotating the refractor plate. In the case of the Barringer instrument the usual spherical aberration and defocussing of a wide angle interferometer are present, and in addition there is astigmatism. However the use of high refractive index slabs results in acceptable fringe visibilities over a few millimeters of delay scanning distance (Zwick et al, 1971). As this scan region can be centred at any pre-chosen delay position it is possible to scan through sufficient independent spectral elements to perform a spectral analysis on the interferogram segment and so to achieve good specificity to supplement the high sensitivity of the field-widened device.

Correlation interferometry is a technique for extracting specific desired information from the radiation interferogram as efficiently as possible, in order to keep to a minimum uncertainties due to all sources. In this case

correlation may be done on interferograms obtained with conventional Fourier instruments such as the Block spectrometer, or a set of pre-determined weights (correlator) may be used which are applied to the interferograms in real time with rather simple hardware.

3.3.2 Optical Arrangement

The basic configuration for a correlation interferometer is shown in Figure 8. Operation of the instrument consists of varying the interferometer delay by either moving one of the end mirrors or by rotating the scanning refractor plate. The latter technique offers great simplicity in comparison to scanning of one of the end mirrors, as there is no possibility of spoiling the alignment by tilt effects. The scan is monitored by a reference interferogram and by means of an encoder fixed to the scanning plate. Ordinary interferometers scan through zero delay whereas the refractively scanned device merely uses the encoder pulse to sense the beginning of the scan. A filter is used to isolate the spectral region of interest. If several separate regions are of interest, multiple detectors may be used to advantage in conjunction with dichroic beamsplitters and spectral filters.

3.3.3 Signal Processing

Processing of the resultant signal is carried out in two stages. In the first stage, fringes from the reference source are used to heterodyne the high frequency carrier present in the signal while at the same time automatically compensating for small irregularities in the scan or drifts in the optical paths.

In correlation interferometry a very high degree of specificity is obtained from the resulting preprocessed signal by the application of a linear digital filter. This filter consists of a set of weights chosen in such a manner as to provide an output which measures quantitatively the presence of a specific spectral signature, but which is insensitive to the interfering spectral signatures. This filter may simultaneously be optimized for the rejection of various types of synchronous and non-synchronous noises. Appendix B outlines the relationship between the the spectra and the interferograms, while Appendix C describes the mathematical

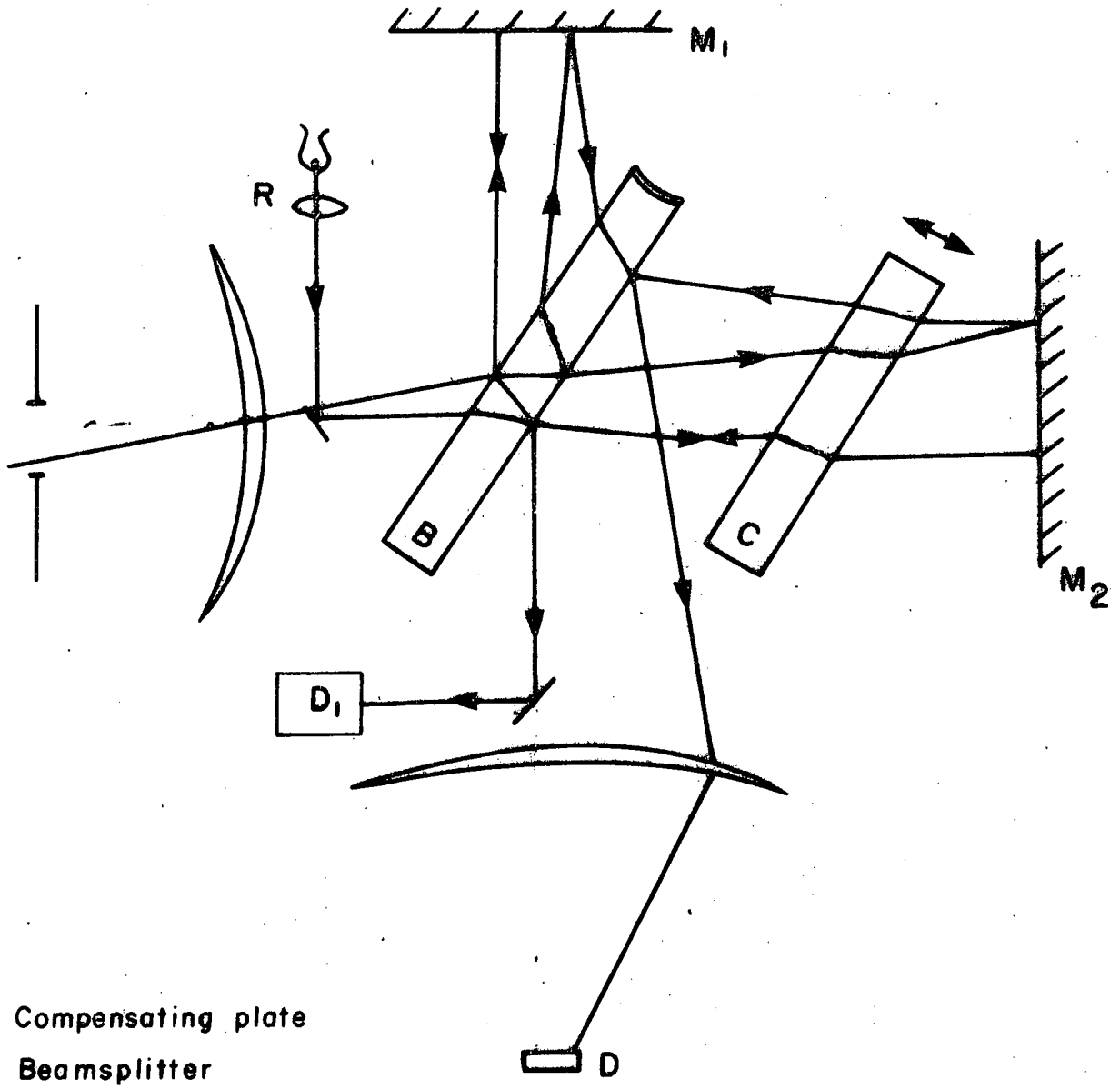

C	Compensating plate
B	Beamsplitter
D	Signal detector
D_1	Reference detector
R	Reference source
M_1 M_2	Mirrors

Figure 8. OPTICAL LAYOUT OF AN INTERFEROMETER

techniques for selecting the weighting functions. In setting up for operation, sample interferograms are observed for as wide a range of interferent conditions as is considered probable under operation conditions. The techniques of Appendix C are then used to determine the weighting function(s).

One powerful feature of the technique is its capability for economically measuring several different signatures whenever these provide information over overlapping regions of the interferogram, simply by the simultaneous application of different weighting functions. In cases where the signatures occur in different spectral regions, separation prior to the detector as mentioned above eliminates crosstalk between outputs; however where crosstalk is not a problem the radiation may be received by a single detector.

A somewhat emperical approach will be used to express the S/N response of an interferometer sensor for HCl detection. The methods used to evaluate noise in Fourier spectroscopy are reviewed in James and Steinberg (1969). Basically the difficulty is that the detector receives all of the radiant energy all of the time (true multiplex advantage) but the time varying component is only that of the Fourier transform of the spectral radiance at the given delay and scan rate. The detector noise is fixed and easily evaluated but noise due to radiance changes (multiplex disadvantage) are indeed difficult to express.

A signal response is therefore here evaluated as an average value over the interferogram correlation region. A modulation efficiency, m, is derived from computed interferograms, and is defined as

$$m = \frac{\langle I^g(X) \rangle - \langle I^i(X) \rangle}{I^g(0) - I^i(0)} \qquad (14)$$

Where I(X) is the interferogram value at the delay region X, < > denotes average value, and g and i refer to the interferograms when HCl vapour is included and when it is not included respectively. Values of m were evaluated directly from the interferograms.

Once these modulation efficiences are defined one can write the response due to HCl vapour by using equations 6 and 14, and including the interference filter,

$$S = A\Omega\tau_o m \left[\int (N_\nu^i(S) - N_\nu^g(S)) . F \, d\nu \right] . \tag{15}$$

Values of $N_\nu(S)$ and $N_\nu^g(S)$ for the downward looking mode are obtained readily from equation 1 and in the case of interferents only $TR_\nu(S) = TR_\nu^i(S)$ where as for the case including HCl the transmittance becomes $TR_\nu(S) = TR_\nu^i(S) . TR_\nu^g(S)$.

In the downward mode, but using ground chopping the response is

$$S^{gc} = m.A\Omega\tau_o \left[\int c \, T_{R_\nu}^i(S) \, (1 - TR_\nu^g(S)) . F_\nu \, d\nu \right] \tag{16}$$

Where, as before, C was set equal to 10% of $\varepsilon_E B_\nu(T_E)$, the earth's average spectral radiance.

Finally the upward looking response is (from equations 4 and 15)

$$S^u = mA\Omega\tau_o \left[\int B_\nu(T_A) \, TR_\nu^i(S) \, (1 - TR_\nu^g(S)) \, F_\nu \, .d\nu \right] \tag{17}$$

These response signals were computed for various HCl burdens, and for differing interferent transmittances. In addition the response was compared with response due to detector noise as given by equation 7.

The results of the calculated response signals is given in the next section, and the programmes used are described in Appendix D. Some work was done to evaluate the best region of the interferogram to perform the HCl detection. The criteria chosen was to find the region which gave the optimum sensitivity but at the same time, the best specificity. It was found that scanning the .065 to 0.1 mm delay region gave the best results. The choice of region was not especially critical so that slight changes in the choice of operating region did not severely change the results (provided that weighting functions were derived for that region). Approximately equal sensitivity would be achieved without the weighting function correlation, but not nearly such good interferent rejection could be possible.

The interferometer parameters were as follows:

$$A\Omega = 1.1 \times 10^{-1} \text{ cm}^2 \text{ Sr}$$
$$\tau_o = 0.06$$
$$A_d = 0.16 \text{ cm}^2$$
$$D^* = 10^{11} \text{ cm Hz}^{1/2} \text{ W}^{-1}$$
$$\Delta f = 1 \text{ Hz}$$

3.4 CORRELATION GAS CELL ANALYZER

The non-dispersive infrared gas cell analyzer has been in use for many years. Luft (1943) first constructed such a device and a succession of workers have since used similar systems (Martin, 1953; Smith and Pidgeon, 1963; Goody, 1968; Ludwig et al, 1969). The basic theory of operation of these instruments is identical, the differences being in the optical arrangement of the components, the methods used for modulating the incoming signal and the electronic signal processing. Commercial instruments have been developed by General Dynamics and Barringer Research Limited, and perhaps others.

Figure 9 shows the basic layout of one such correlation gas cell analyzer system. The incident radiation is divided at the beamsplitter and passes through one or the other of two gas cells, C1 or C2 and onto one of the detectors. One of the gas cells (C1 say) contains a sample of the same type of gas as is to be sensed, while the other contains a spectrally inactive gas. The optimum amount of gas is experimentally (or computer) evaluated to give maximum response. (In another version of this instrument the radiation is alternately passed through cells C1 and C2 and onto a common detector.)

At a wavelength where the gas absorbs strongly, radiation passing through cell C2 (containing no target gas) is attenuated depending on the quantity of target gas that the radiation has passed through before reaching the instrument. However when the target vapour radiation passes through C1, the radiation is largely removed regardless of the amount of gas prior to the instrument. In this path it is much less affected by the quantity of target gas prior to the cell.

A chopper is used to modulate the input source radiance to a frequency best suited to the detector (in the 3 k Hz region for cooled PbS). The chopper also chops an additional source whose purpose is to provide a synchronous signal to be used in a product detector for synchronous monitoring of the source radiance at each detector. The difference in the output from these two synchronous source signals is an output which varies in a manner indicative of the amount of target vapour signature at the sensor. The signal processing is shown in a block diagram form in Figure 10.

Normally the two detector responses would vary with ambient changes in responsivity as the two detectors age, change temperature, etc. Further the response could depend to some extent on the thermal stability of the two arms of the instrument. To help remove these undesirable effects

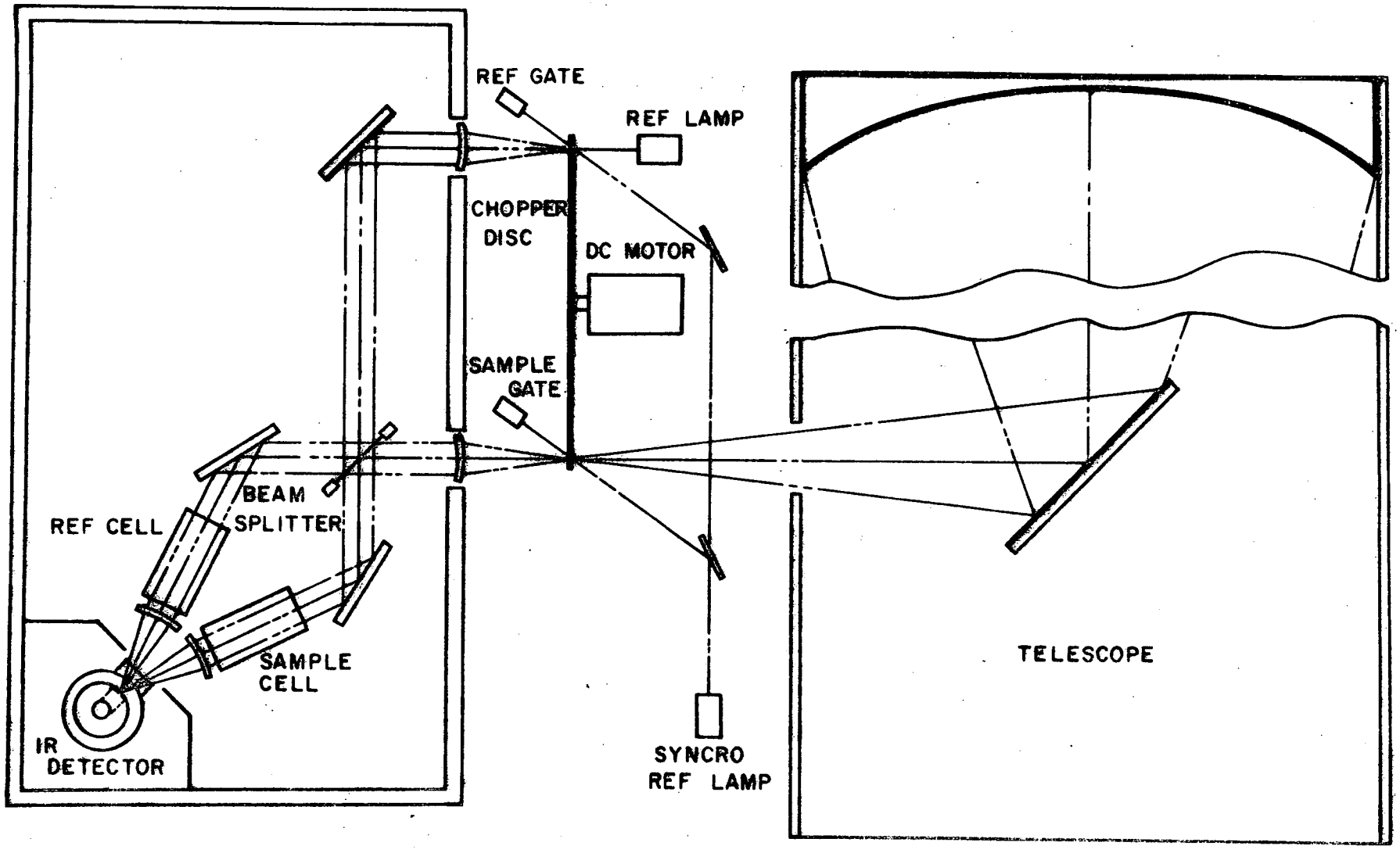

CORRELATION GAS CELL ANALYSER FIGURE 9.

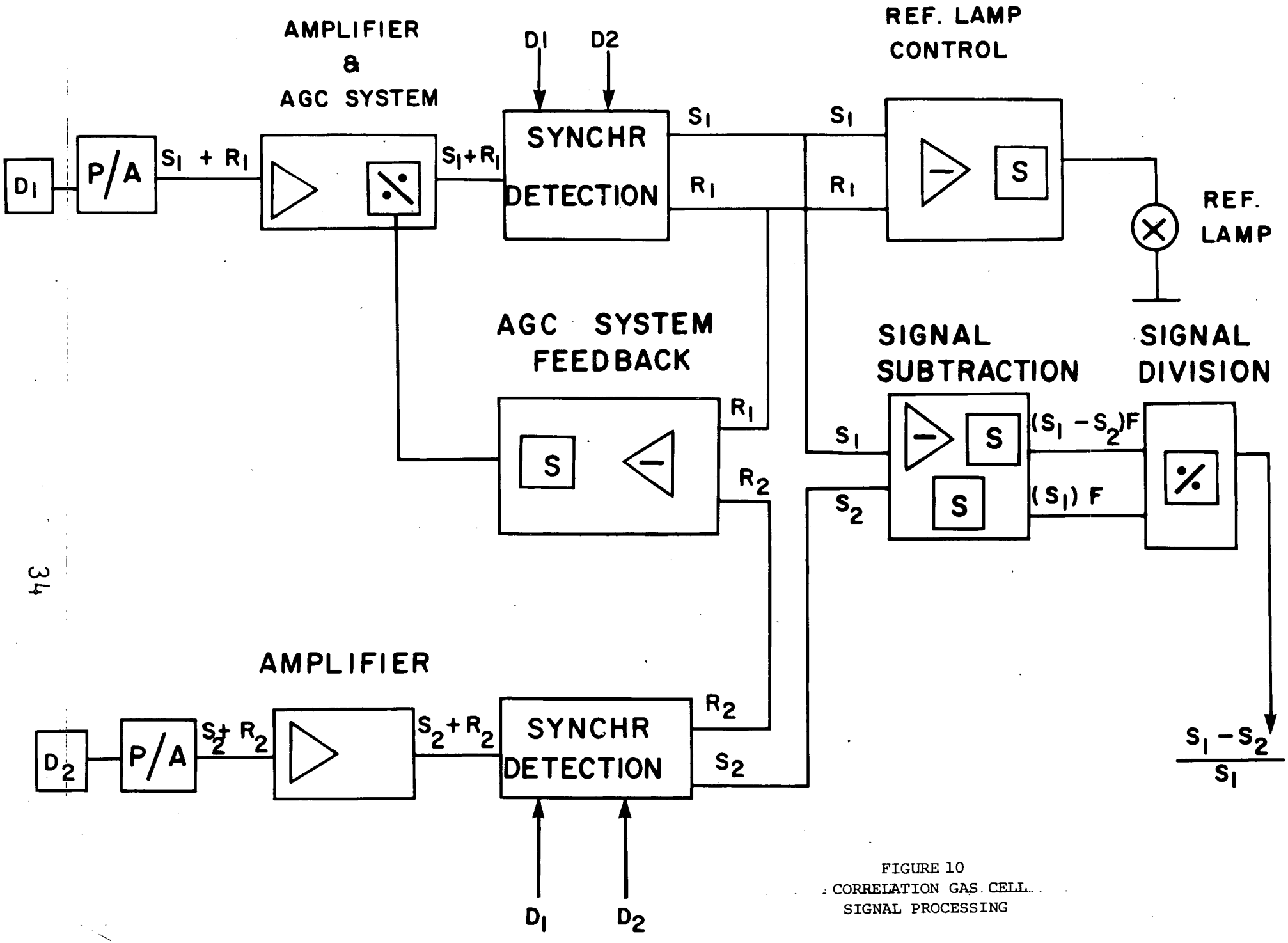

FIGURE 10
CORRELATION GAS CELL
SIGNAL PROCESSING

a reference lamp is included in the system. The detector then senses both the source and the reference lamp. Another signal, synchronous with the reference lamp is used to synchronously extract the reference lamp response from each detector and the difference between the two detector reference lamp responses is held constant by a feedback loop, which adjusts the gain of one detector.

In this way the two detector responses are forced to "track" each other. In the case where the radiation is alternately passed through C1 and C2 to a common detector, the optical paths may be forced out of balance by thermal emission changes in the two optical paths, or dust specks etc. The two detector forced tracking system eliminates these effects. An additional feedback loop is used to keep the average reference lamp radiance equal to the average source radiance so that differences due to changing detector responses with input power are minimized.

The correlation gas cell analyzer has a high degree of specificity since absorption of radiation at wavelengths other than those absorbed by the target gas affect both outputs equally, and so does not affect the difference. Rejection of interferents is very good when both target and interferent gases have a large ratio of line separation to line width as in the HCl case. Laboratory work by Bartle et al (1971) has demonstrated the rejection capability of a correlation gas cell analyzer.

The output signal from a correlation gas cell analyzer may be written from equation 6:

$$S = A\Omega\tau_o \int_\nu (N_\nu(S)\ \tau_{c1} - N_\nu(S)\ \tau_{c2})\, d\nu$$

where τ_{c1} is the normalized transmittance through cell C1 and τ_{c2} the

transmittance through cell C2. τ_{c1} was obtained from a radiative transport calculation through a cell 2 cm long containing 0.1 atmospheres of HCl cell τ_{c2} was set equal to 1. The signal duty cycle (time during which source is being sensed) is included in the calculations.

The values for source radiance at the receiver $N_\nu(S)$ were obtained as before from equations 1, 2, 3, and 4.

The correlation gas cell analyzer parameters used in the computations presented in the next section were,

$$A\Omega = 0.1 \text{ cm}^2 \text{ Sr}$$
$$\tau_o = 0.1$$
$$A_d = 0.16 \text{ cm}^2$$
$$D^* = 10^{11} \text{ cm Hz}^{1/2} \text{ W}^{-1}$$
$$\Delta f = 1 \text{ Hz}$$

In evaluating the signal to noise ratio for the double element detector system the noise equivalent power expressed by equation 7 can be used, but a factor of $\sqrt{2}$ is required to account for the rms addition of the two individual detector noises when the signal difference is formed.

Section 4

SENSOR TRADE-OFFS FOR HCl DETECTION

4.1 HCl SENSOR DETECTION SENSITIVITY

Results of the computation outlined in sections 3.2, 3.3 and 3.4 for the three optical correlation instruments are given in Table I. The cases evaluated are:

(a) upward looking geometry using a computed HCl transmittance, and Migeottes spectral transmittance of the whole atmosphere.

(b) a downward looking configuration which employs ground chopping. In this case only the HCl transmittance was considered, as it is not necessary to look through an atmospheric amount of interferent vapour in this case. The ground chopping radiance is taken to be 10% of the surface average radiance.

Two different integrated amounts of HCl were evaluated; these correspond to a 0.5 ppb HCl concentration over a 2 km pathlength (1 ppm-m) and a 50 ppb concentration over a 2 km pathlength (100 ppm-m).

As expected, the response is not quite linear, although at these low concentrations the non-linearity is rather small.

It was beyond the scope of this work to evaluate the response at very large burdens of pollution. It is expected that useful measurements of integrated burdens of several orders of magnitude more HCl (thousands of ppm-m) are readily achievable.

The conclusions from the table are that the gas cell analyzer is the most sensitive device, followed by the interferometer and the least sensitive device is the correlation spectrometer. It is possible that the geometrical parameters for these instruments could be changed so that the numbers would be changed somewhat. However, the parameters in the calculation are those of existing hardware devices. Changes by factors of 2 are possible, but orders of magnitude changes would be rather difficult.

Instrument	Operating Mode	HCl Vapours and Interferents	Computed S/N (Assuming Detector Noise And and 1 HZ Bandwidth)
Correlation Gas Cell Analyzer	Vertically Upward	1 ppm-meter HCl and Migeotte Transmittance	0.6
	Vertically Upward	100 ppm-meters HCl and Migeotte Transmittance	53
	Downward with Ground Chopping	1 ppm-meters HCl No interferents	0.13
	Downward with Ground Chopping	100 ppm-meters HCl No interferents	12
Correlation Interferometer	Vertically Upward	1 ppm-m HCl and Migeotte Transmittance	6.3×10^{-2}
	Vertically Upward	100 ppm-m HCl and Migeotte Transmittance	8.1
	Downward with Ground Chopping	1 ppm-m HCl no interferents	—
	Downward with Ground Chopping	100 ppm-m HCl no interferents	3.6
Correlation Spectrometer	Vertically Upward	1 ppm-m HCl and and Migeotte Transmittance	1.5×10^{-2}
	Vertically Upward	100 ppm-m HCl and Migeotte Transmittance	1.4
	Downward with Ground Chopping	1 ppm-m HCl no interferents	3.4×10^{-3}
	Downward with Ground Chopping	100 ppm-m HCl no interferents	3.1×10^{-1}

TABLE I

HCl SENSITIVITY OF OPTICAL CORRELATION INSTRUMENTATION

The sensitivity advantage of the correlation gas cell analyzer stem mainly from two factors. Firstly, the average optical transmission is approximately two times greater than the interferometer as the latter device returns half the radiance back to the source. Secondly, the gas cell device modulates all wavelengths in phase whereas the interferometer working at an interferogram HCl peak response has some of the signal (especially here were isotopes exist) out of phase.

4.2 HCl SENSOR SPECIFICITY

The computed effect of interferent changes were performed by evaluating the instrument response changes which resulted when the same 1 ppm-m of HCl was present, but when the interferent spectrum changed. The change in interferent spectrum was arbitrarily chosen to be that which results in an atmospheric transmittance which is the square root of the Migeotte atlas transmittance. This should be very crudely equivalent to an air mass change of 0.5.

This spectrum was not chosen so much because of its relationship to the real physical world, but rather because of ease of evaluation. Since this same interferent spectrum was presented to each sensor it gives some indication of the specificity of each sensor. The results of this computation are presented in Table II.

As seen from Table II, the interferometer is by far the most specific of the sensors evaluated. This result is due to the fact that the weighting function correlator is computed so as to give the minimum offset, in the rms sense, to a given library set of interferograms. If the library set of conditions brackets (or even better includes some of) the range of interferent changes encountered, then they are "anticipated" interferents and can be very effectively discriminated against.

The other two sensors (spectrometer and the gas cell analyzer) have fixed correlating functions; a metal disc or mask in the case of the spectrometer, and an HCl gas cell in the other case. These fixed correlator functions are reasonably good at discriminating against interferent effects, but not as good as the interferometer.

4.3 SENSOR SIZE, WEIGHT, COST AND COMPLEXITY

A ballpark estimated cost for fabricating each of the three optical sensors for HCl detection is shown in Table III, along with some size, weight and relative complexity figures. These are estimated costs.

4.4 THE BEST HCl SENSOR

As has been shown in Sections 4.1, 4.2 and 4.3 the best sensor for HCl detection depends on the criterion chosen. The correlation gas cell analyzer has the best sensitivity, but the interferometer has the best specificity and the spectrometer has perhaps the best ruggedness.

If the gas cloud can be monitored from a ground based mobile van with the sensor pointed in the upward direction, the interferometer would be recommended. The great specificity of this sensor is valuable because the ground cloud plume may contain a great many interferent species. The time available for burden measurement from a low speed surface vehicle could be reasonably long (say 1 second) and the plume could be mapped by elevation scanning and by van mobility.

The correlation gas cell analyzer has good sensitivity however, and seems somewhat better if the HCl cloud is to be monitored to the lowest possible detectable amounts. In this case the need for high interferent rejection has been sacrificed for the gain in sensitivity.

If the HCl cloud is to be monitored by looking downward from the airborne platform it will either be necessary to observe when the atmosphere has a known temperature different from the earth's surface, or else possibly employ the fluctuations in source radiance from the earth's surface. If the sensor footprint moves quickly so as to obtain large area coverage from a quickly moving platform, the fast response time achievable with the correlation gas cell analyzer would be useful. The alternative is to use image motion compensation techniques which would add complexity and cost to the system.

Instrument	Operating Mode	Spectral Change	Equivalent HCl Response
Correlation Gas Cell Analyzer	Vertically Upward	1 ppm-m HCl with Migeotte Spectrum, changed to 1 ppm-m HCl with square root of Migeotte Transmittance ≈ 0.5 air mass	≈ 15 ppm-m HCl
Correlation Spectrometer	Vertically Upward	as above	≈ 20 ppm-m HCl
Correlation Interferometer	Vertically Upward	as above*	≈ .04 ppm-m HCl

* The linear digital filter weighting function was in this case evaluated from Migeottes atlas transmittance, and from cube root of Migeottes atlas transmittance. The optimum filter from this spectral set was applied to the case where the interferent spectrum corresponds to the square root of Migeottes atlas.

TABLE II

OUTPUT CHANGES DUE TO INTERFERENT EFFECTS

Instrument	Size	Weight	Cost*	Relative Complexity	Ruggedness
Gas Cell Analyzer	2' x 2' x 8" plus 3' telescope	50 lbs	$32,000.00	Moderate	Moderate
Correlation Interferometer	18" x 12" x 12" plus 3' telescope	30 lbs	$65,000.00	High	Moderate
Correlation Spectrometer	2' x 1' x 8"	30 lbs	$30,000.00	Moderate	Moderate-high

* ESTIMATE ONLY BARRINGER RESEARCH SENSORS

TABLE III

HCl SENSOR PARAMETERS

REFERENCES

Armstrong, B.H., and Nicholls, R.W., "Emission, Absorption and Transfer of Radiation in Heated Atmospheres", Pergamon Press (1972).

Bell, R.J., Introductory Fourier Transform Spectroscopy, Academic Press (1972).

Barringer, A.R., Schock, J.P. Proc. 4th Symposium, Remote Sensing of the Environment, 779 (1966).

Bartle, E.R., Meckstroth, E.A., Kayo, S., General Dynamics Report AFRPL-TR-71-59 (1971).

Cann, M.W.P., Nicholls, R.W., Conf. on Atmos. Radiation, Fort Collins, August (1972).

Connes, P., J. Phys. Radium, 19, 262 (1958).

Davies, J.H., Correlation Spectroscopy, Anal. Chem. 42, 101A, (1970).

Decker, R.N., Harivet, M.D., Apl. Optics 7, 2205 (1968).

Dick, R., Levy, G., Aspen International Conference on Fourier Spectroscopy, Aspen (1970).

Elterman, L., Vertical Atten. Model with 8 Surface Meteorological Ranges 2 to 13 km., AFCRL 70-0200.

Goody, R., Cross-Correlating Spectrometer, J.O.S.A., 58, 900 (1968).

Grenda, R.N., Bortner, M.H., LeBel, P.J., Dick, R., Davies, J.H., AIAA Paper #71-1120 Palo Alto, November (1971).

Hansen, G., Z. Instrumentenkunde, 61, 411 (1941).

Hodges, J.A., Applied Optics 11, 2304 (1972).

Ibbett, R.N., Aspinall, D., Grainger, J.F., Applied Optics 7, 1089, (1968).

James, J.F., Sternberg, R.S., The Design of Optical Spectrometers, Chapman and Hall (1969).

Ludwig, C.B., et. al, Rem. Sens. of Atm. Envir. General Dynamics Report GDC-ERR-1317 (1968).

Ludwig, C.B., Bartle, R., Griggs, M., Study of Air Pollutant Detection by Remote Sensors, NASA Report CR1380 (1969).

Luft, 1943, referenced in Infrared Physics, by J. Houghton and S.D. Smith, Oxford Press (1966) p. 277.

Martin, Research 6, 172 (1953).

Millan, M., Townsend, S., Davies, J.H., Study of Barringer Remote Sensor, University of Toronto Report 146, (1969).

Millan, M.M., PhD Thesis, University of Toronto (1971).

McClatchey, R.A., Fenn R.W. Selby J.E.A., Vol 3, F.E. Garing, J.S., Optical Properties of the Atmosphere, Third Edition", AFCRL 72-0497 (1972).

Moffat, A.J., Robbins, J.R., Barringer, A.R., Atm. Envir. 5, 511 (1971).

Migeotte, M., Nevin, L., Swensson, The Solar Spectrum from 2.8 to 23.7 microns, Part 1 Photometric Atlas, University of Liege, Contract AF61(514) 432.

Nelson, E.D., Fredman, M.L., Hadamard Spectroscopy, J.O.S.A. 60, 1664 (1970.

Necomb, G., Millan, M., Theory, Applic. and Results of the Long Line Correlation Spectrometer, IEEE Geoscience Electronics, 8, 149 (1970).

Steel, W.H., Interferometry, Cambridge University Press (1967).

Smith, S.D., Pidgeon, C.R., Proc. XII Int. Symp. Liege June (1963).

Wolfe, W.L., Handbook of Military Infrared Technology, ONR, Washington (1965).

Williams, D.T., Kolitz, D.L., Apl. Optics 7, 607 (1968).

Zwick, H.H., Dick, R., Davies, J.H., Barringer Research Report TR71-167.

Zwick, H.H., Shepherd G.G., Applied Optics 10, 2569 (1971).

Zwick, H.H., Millan, M., Can. Aeron. Sp. Journal 17, 413 (1971).

APPENDIX A

Radiative Transport

In the thermal infrared spectral region the transmission of radiation through the atmosphere is attenuated due to absorption by atmospheric gases and aerosols, and due to scattering by airborne particulate matter. In addition however there is a competing emission from the gases and aerosols which tends to offset the absorption radiance losses. One may express (Armstrong and Nicholls, 1972) the change in radiance $dN_\nu(S)$ as follows:

$$dN_\nu(S) = -N_\nu(O)\, d\tau + J_\nu(S)\, d\tau$$

where $d\tau = k_\nu \rho\, ds$ is the element of optical depth, k_ν is the mass absorption coefficient, ρ the density, ds the element of path length. The mass absorption coefficient depends on the molecular parameters, and on the atmospheric temperature, pressure and composition.

$J_\nu(S)$ is the source function and is given by $J_\nu(S) = j_\nu(S)/k_\nu$ and $j_\nu(S)$ is the mass emission coefficient. When this expression is integrated the formal solution is

$$N_\nu(S) = N_\nu(O)\exp\left(-\int_o^S k_\nu \rho\, ds\right) + \int_o^S J(S')\exp\left(-\int_{S'}^S k_\nu \rho\, ds\right) ds'$$

The first term on the right is the decrease in radiance due to atmospheric extinction, and the second term is the increase due to emission and scattering.

The source term is very difficult to evaluate for a scattering atmosphere since it is necessary to completely characterize the aerosol and radiating sources in order to perform the geometric scattering function integration.

For a non-scattering atmosphere the emission coefficient is considerably simplified, and can be written simply as

$$j_\nu(S) = k_\nu(S)\, B_\nu(T)$$

When $B_\nu(T)$ is the plank radiance function describing a black body at temperature T.

In the usual atmospheric temperature case, where one does not have induced emission, the transmission function approach is a convenient method of evaluating spectral emissivity ε_ν of the atmosphere,

$$T_\nu(S) = 1 - \varepsilon_\nu = 1 - \frac{N_\nu(S)}{B_\nu(T)}$$

If for the moment one neglects the radiance $N_\nu(O)$ into the gas layer, and assumes an isothermal atmosphere

$$T_\nu(S) = 1 - \int_O^S \exp\left(-\int_{S'}^S k_\nu \rho \, ds\right) ds'$$

$$= \exp\left(-\int_O^S k_\nu \rho \, ds\right)$$

Hence one may write,

$$N_\nu(S) = N_\nu(o)\, Tr_\nu(S) + (1 - Tr_\nu(S))\, B_\nu(T)$$

APPENDIX B

RELATION BETWEEN RADIATION SPECTRUM AND INTERFEROGRAM

In this section the relationship between the spectrum of the radiation incident upon an interferometer system, and output of the system will be outlined.

Incident Radiation

The radiation incident at the instrument will have a dependence with spectral frequency which may be conveniently represented

$$S(\nu, \bar{Q}) = S_o \times T(\nu, \bar{Q}).$$

The vector $\bar{Q}$ has been used to represent all the parameters which determine the detailed structure of the spectrum; things such as quantities and profiles of various absorbers along the optical path, temperature pressure structure along the path, gradient of any non-flat reflectors: (in short, anything which results in structure). The results of all such parameters may be considered as a dimensionless transmission factor $T(\nu,\bar{Q})$. The received spectral radiance S and the background radiance S_o on the otherhand have dimensions of [watts/cm^2 sterad. wavenumbers].

Defined in this manner, S is independent of the interferometer system. However, it is convenient to include in $\bar{Q}$ the characteristics of any spectral filter used in the instrument to isolate the region of interest in the spectrum. Thus T will include the filter transmission function.

INTERFEROMETER OUTPUT

The remainder of the interferometer system is characterized by its light grasp or etendu E (cm^2 steradians), its efficiency e (dimensionless) and of course the delay setting x (centimeters). (The efficiency e may be used to account for variation in x over the interferometer aperture by including a fringe visibility term.) For a given setting of the interferometer, the radiation available to the detector is

$$I(x, \bar{Q}) = e\,E \int_{\nu=0}^{\infty} [1 + \cos(2\pi\nu x)]\, S(\nu,\bar{Q})\,d\nu$$

$$= e\,E\,S_o \left[\int_{\nu=0}^{\infty} T(\nu,Q)\,d\nu + \int_{\alpha}^{\infty} \cos(2\pi\nu x)\, T(\nu,Q)\,d\nu\right]$$

We may define $P_o = e\,E\,S_o$ (nominal available spectral power, [watts/wavenumber]), and

$$W(x,\bar{Q}) = \int_{\nu=0}^{\infty} \cos(2\pi\nu x)\, T(\nu,Q)\,d\nu$$

(equivalent width of optical path + interferometer system for delay setting x, in wavenumber).

Then $I(x,\bar{Q}) = P_o\,[W(0,\bar{Q})]$ (watts).

The equivalent widths $W(x,\bar{Q})$ depend only on the characteristics of the optical path and the spectral filter, and may be evaluated independently of considerations of the gross parameters S_o, e, and E.

Expansion of Spectrum

It is generally desired to operate under a range of conditions for $\bar{Q}$. Signal processing will have as its object the measurement of one or more of the parameters comprising $\bar{Q}$, in such a manner as to be insensitive to variation of the remaining parameters within their anticipated range. In developing a procedure for making this measurement it is useful to consider approximations for the variation of the spectra and interferograms with the parameters $\bar{Q}$.

If nominal conditions are defined by parameters $\bar{Q}_o$, it is possible to write

$$S(\nu,\bar{Q}) = S(\nu,\bar{Q}_o) + \Sigma(Q_i - Q_{oi})\ S_i(\nu) + \ldots\ldots\ldots\ldots$$

$$= S_{oo}(\nu) + \Sigma\ q_i\ S_i(\nu) + \Sigma\ q_i q_j\ S_{ij}(\nu) + \ldots\ldots$$

Where, if the terms of such an expression are obtained from a Taylor expansion, one has

$$S_i = \left[\frac{\partial S(\nu,\bar{Q})}{\partial\ Q_i}\right]\ \bar{Q}_o$$

$$S_{ij} = \left[\frac{\partial^2 S(\nu,\bar{Q})}{\partial Q_i \partial Q_j}\right]\ \bar{Q}_o$$

etc.

In the case of Q_i representing the concentration path products for absorber with absorption coefficients α_i, one has

$$S(\nu,\bar{Q}) = S_o e^{-\Sigma Q_i \alpha_i}$$

$$= S_o e^{-\Sigma Q_{io} \alpha_i}\ [1 - (\Sigma q_i \alpha_i) + (\Sigma q_i \alpha_i)^2/2! \ldots\ldots\ldots]$$

$$= S_{oo} + \Sigma\ q_i\ S_i + \ldots\ldots\ldots$$

This gives

$$S_{oo} = S_o e^{-\Sigma Q_{io} \alpha_i}$$

and $\quad S_i = S_{oo}\ \alpha_i$

Expansion of Interferogram

Because of the linear property of fourier transformation, any expansion of the spectrum as a sum of components results in an interferogram which is the sum of the interferograms of the individual spectral components.

Thus,

$$S(\nu,\bar{Q}) = S_{oo}(\nu) + \Sigma\, q_i\, S_i(\nu) + \Sigma q_i q_j\, S_{ij}(\nu) + \ldots\ldots$$

gives an interferogram

$$I(x,\bar{Q}) = I_{oo}(x) + \Sigma\, q_i\, I_i(x) + \Sigma\, q_i q_j\, I_{ij}(x) + \ldots\ldots$$

where $I_{oo}(x) = \int_{\nu=0}^{\infty} [1 + \cos\,(2\pi\nu x)]\; S_{oo}(\nu)d\nu$.

It is instructive to consider the case where only the linear terms are important. If there are m parameters q_i $(i = 1, \ldots m)$, and if the interferograms is observed at n points x_K $(K = 1, \ldots n)$, then the observations are

$$\begin{aligned} I(x_1) &= I_{oo}(x_1) + q_i\, I_1(x_1) \;\ldots\ldots + q_m I_m(x_1) \\ &\vdots \qquad\quad \vdots \qquad\quad \vdots \qquad\qquad\quad \vdots \\ I(x_n) &= I_{oo}(x_n) + q_1 I_1(x_n) \;\ldots\ldots + q_m\, I_m(x_n) \end{aligned} \quad .$$

If there are just m observation points, and if the I_{oo} terms are known, then the observations consititute m equations in m unknown (the q_i), and may be solved by matrix inversion. The equations may be written

$$I(x_k) = I_{oo}\,(x_k,\bar{Q}) = \sum_{i=1}^{m} q_i\, I_i(x_k)$$

$$= \Sigma\, q_i\, I_{ik}$$

which have the solutions

$$q_i = \sum_{k=1}^{m} I_{ik}^{-1}\, [I(x_k) - I_{oo}\,(x_k,\, \bar{Q})] \quad .$$

In the case that there are more observation points than there are variables, the linear least squares technique could be applied.

APPENDIX C

DETERMINATION OF WEIGHTING FUNCTIONS

Basic Principles

In the linear approximation, it may be assumed that the interferogram may be represented in terms of the interferogram obtained for some nominal set of conditions (nominal atmospheric parameters and nominal composition), to which is added differential interferograms according to the deviations of the conditions from nominal. For example if the parameters which determine the spectral distribution of the incident light are represented by some array of values $\bar{Q}$, i.e.

$$S = S(v, \bar{Q}), \quad (\bar{Q} = Q_1, Q_2, \ldots Q_N)$$

then at least for small deviations of $\bar{Q}$ from some nominal set of values $\bar{Q}_o$ we may write

$$S(v, \bar{Q}) \simeq S(v, \bar{Q}_o) + \sum_1^N q_i (dS/dQ_i)_{\bar{Q}_o}$$

$$\equiv S(v,\bar{Q}_o) + \Sigma q_i S_i(v),$$

where $q_i = Q_i - Q_{io}$.

Now the interferogram observed $I(x,\bar{Q})$ is the cosine fourier transform (CFT) of $S(v,\bar{Q})$. As Fourier transformation is a linear operation, we may write to the same approximation

$$I(x,\bar{Q}) \simeq I(x,\bar{Q}_o) + \sum_1^N q_i I_i(x),$$

where $I_i(x)$ are the CFT's of $S_i(v)$.
(Non=linear effects may be included by adding terms of the form $q_i q_j I_{ij}(x)$).
It is desired to measure one of the parameters, Q_j say. Unfortunately variation of the other parameters from nominal values as well as this one result in variation of the interferogram. The problem is to make a measurement on the interferogram which is sensitive only to variations in the target parameter, q_j, and not to the othe q_i.

Signal processing theory has dealt with the application of a linear filter. or weighting function H(x) to the interferogram to make the measurement. An additional degree of freedom may be available in the length of time D(x) (duration) spent at each interferogram point (D(x) must be positive). The measurement made is then

$$M(\bar{Q}) = \int H(x)\ D(x)\ I(x,\bar{Q})dx$$
$$= M_o + \Sigma q_i\ M_i;$$

where $M_i = \int H(x)\ D(x)\ I_i(x)\ dx,$
$M_o = \int H(x)\ D(x)\ I(x,Q_o)dx.$

It is relatively simple to produce a weighting function which gives zero for all the M_i, except for the target M_j. It is only necessary the the range of x considered contains at least as many points which exhibit different variation (with the parameters $\bar{Q}$) as there are parameters. This requires that the matrix B_{ij}

$$B_{ij} = \int I_j(x)\ I_j(x)dx$$

be non singular.

The wide degree of freedom remaining in the choice of a filter function (after requiring $M_i = 0$ for $i \neq j$) may be used to minimize the noise or uncertainty obtained in making the measurement.

Representation of Noise

The noises can be divided into four groups, according to whether they are random in time, or synchronous with the scanning of the interferometer delay, and according to whether they are basically additive or multiplicative in their affect on the interferometer output. The table below gives examples of sources for the various noises.

	Random:	Synchronous
Additive:	1. Detector noise, photon noise;	3. Unanticipated interferents;
Multiplicative:	2. Random vibrations, scintillation;	4. Synchronous vibration, scan sweep rate deviations, incorrect specification of weighting function.

The difference in these noise sources is due to the way in which they affect the measurement. Any point of the interferogram x supplies a contribution to the measurement

$$\Delta M(x) = dM/dx$$
$$= H(x)\ D(x) \Sigma\ q_i I_i(x). \qquad (M = \int \Delta M(x)dx).$$

Associated with this contribution there is an uncertainty, $\Delta N(x)$, which adds in an RMS manner with the uncertainties or noises at all other points to give the total uncertainty.

$$N^2 = \int (\Delta N)^2 dx,$$

For synchronous noises, $\Delta N(x)$ increases directly with the length of time the point is observed (the duration $D(x)$). For non-synchronous noises, ΔN increases only with the square root of D. I.E.

$$\Delta N(x) \propto \begin{cases} D(x) & \text{synchronous noises} \\ D^{1/2}(x) & \text{non-synchronous noises.} \end{cases}$$

In the case of additive noises, ΔN is independent of the signal amplitude, while in the case of multiplicative noises N is proportional to the expected size of the signal at that point:

$$\Delta N \propto \langle I(x) \rangle$$
$$= (\Sigma \langle q_i^2 \rangle I_i^2(x))^{1/2}$$

The notation

$$r^2(x) \equiv \Sigma \langle q_i^2 \rangle I_i^2(x)$$

will be used in representing this portion of the multiplicative noises.

In addition to the factors outlined above, each of the contributors to ΔN is weighted by the full weighting function $H(x)$. The various noises will again add up in an RMS manner; i.e.

$$\Delta N^2(x) = \sum_{k=1}^{4} \Delta N_k^2(x).$$

The table below then shows the way in which the various noise sources contribute to ΔN^2, (apart from constant factors which indicate the total severity of the sources).

Variation of Noise Sources $\Delta N_i^2(x)$

	Random	Synchronous
Additive	1. $H^2(x)D(x)$	3. $H^2(x)D^2(x)$
Multiplicative	2. $H^2(x)D(x)r^2(x)$	4. $H^2(x)\ D^2(x)\ r^2(x)$

If the constant factors are a_i (i = as indicated in the table), then we may write

$$\Delta N^2 = H^2[(a_1 + a_2 r^2)D + (a_3 + a_4 r^2)D^2]$$

$$= H^2 D [G_1(x) + G_2(x)D];$$

where $G_1(x) = [a_1 + a_4 r^2(x)]$

$G_2(x) = [a_3 + a_4 r^2(x)]$.

The total expression for the noise is then

$$N^2 = \int H^2(x) D(x) [G_1(x) + G_2(x) D(x)]dx;$$

where $G_1 = a_1 + a_2 r^2$,

$G_2 = a_3 + a_4 r^2$,

and $r^2 = \Sigma \langle q_i^2 \rangle I_i^2(x)$.

Optimization of M/N

Of the various factors which affect the signal to noise ratio M/N achieved in making measurement, only the weighting function H(x) and the duration function D(x) may be varied in an attempt to optimize the ratio once the basic system has been specified.

It is fairly straightforward to find a weighting function H(x) which is optimum for a specified duration function D(x). This will be outlined now.

It is desired to find a weighting function H(x) which gives

$$M_i = \int H(x)\ D(x)\ I_i(x)dx$$

$$= \begin{matrix} 0 & i \neq 1 \\ 1 & i = 1 \end{matrix}$$

This will give a measurement

$$M = \int H\ D\ \ q_i\ I_i\ dx$$

$$= q_1 .$$

H is to be chosen so as to minimize N^2

$$N^2 = \int [H(x)D(x)]^2 G(x)dx$$

where $G(x) = G_1/D + G_2$

Defining $H'(x) = H(x)D(x)$, the problem is to minimize

$$\int H'(x)^2\ \ G(x)dx = N^2 \qquad (1)$$

$$\text{S.t.} \quad \int H'(x) I_i(x)dx = \delta_{i1} \qquad (2)$$

The equations (2) may be multiplied by Lagrange multipliers m_i and added to equation (1), to require

$$\int H'^2\ G dx + \Sigma m_i \int H'\ I_i dx = \text{minimum} .$$

Varying any particular $H'(x)$ will result in zero variation of this expression when H' is optimized: i.e.

$$\frac{\partial}{\partial H'(x_o)} \left[\int H'^2 G dx + \Sigma\, mi \int H'\, I_i\, dx\right] = 0 \text{ for all } x_o,$$

or $2H'(x_o)\, G(x_o) + \Sigma m_i I_i(x_o) = 0.$

This gives

$$H'(x_o) = \Sigma m_i'\, I_i(x_o)/G(x_o)$$

where $m_i' = -m_i/2.$

The m_i may be determined by substituting for H' in the equations (2) and solving:

$$\int H'(x)\, I_j\, (x)\, dx = \delta_{il}$$
$$= \Sigma m_i \int (I_i\, I_j/G)\, dx$$

or $\Sigma m_i\, A_{ij} = \delta_{jl},$

where $A_{ij} = \int (I_i I_j/G)\, dx$

This set of linear equations has the solution

$$m_i' = \Sigma_j\, A^{-1}_{ij}\, \delta_{jl}.$$

where A^{-1} is the inverse of matrix A.

Thus we may write

$$H'(x) = HD = \Sigma\, A^{-1}_{il}\, I_i(x)/G(x)$$

or $H(x) = \Sigma\, A^{-1}_{il}\, I_i(x)/[G_1 + DG_2]x.$

This H(x) can be shown to be the same one which would be used to find those values of q which give the best fit to an observed interferogram I(x), i.e. those q which minimize

$$\int [I(x) - \Sigma q_i I_i(x)]^2 / N^2(x)\, dx,$$

when $$N^2(x) = G_1(x)/D + G_2(x) = G.$$

The following points should be noted.

- If a given function H(x) is used, function $H_1(x) = CH(x)$ may be used to give a larger measurement $M_1 = cM$; but the signal to noise ratio remains unchanged $(M_1/N_1 = M_1/N_1)$.

- If there are synchronous noises only, $(G_1 << G_2)$, then any combination of H and D which give the same product HD will give the same signal to noise ratio. Increasing observation time in such a case does not improve the signal to noise ratio.

APPENDIX D

COMPUTER MODELLING

System Flow

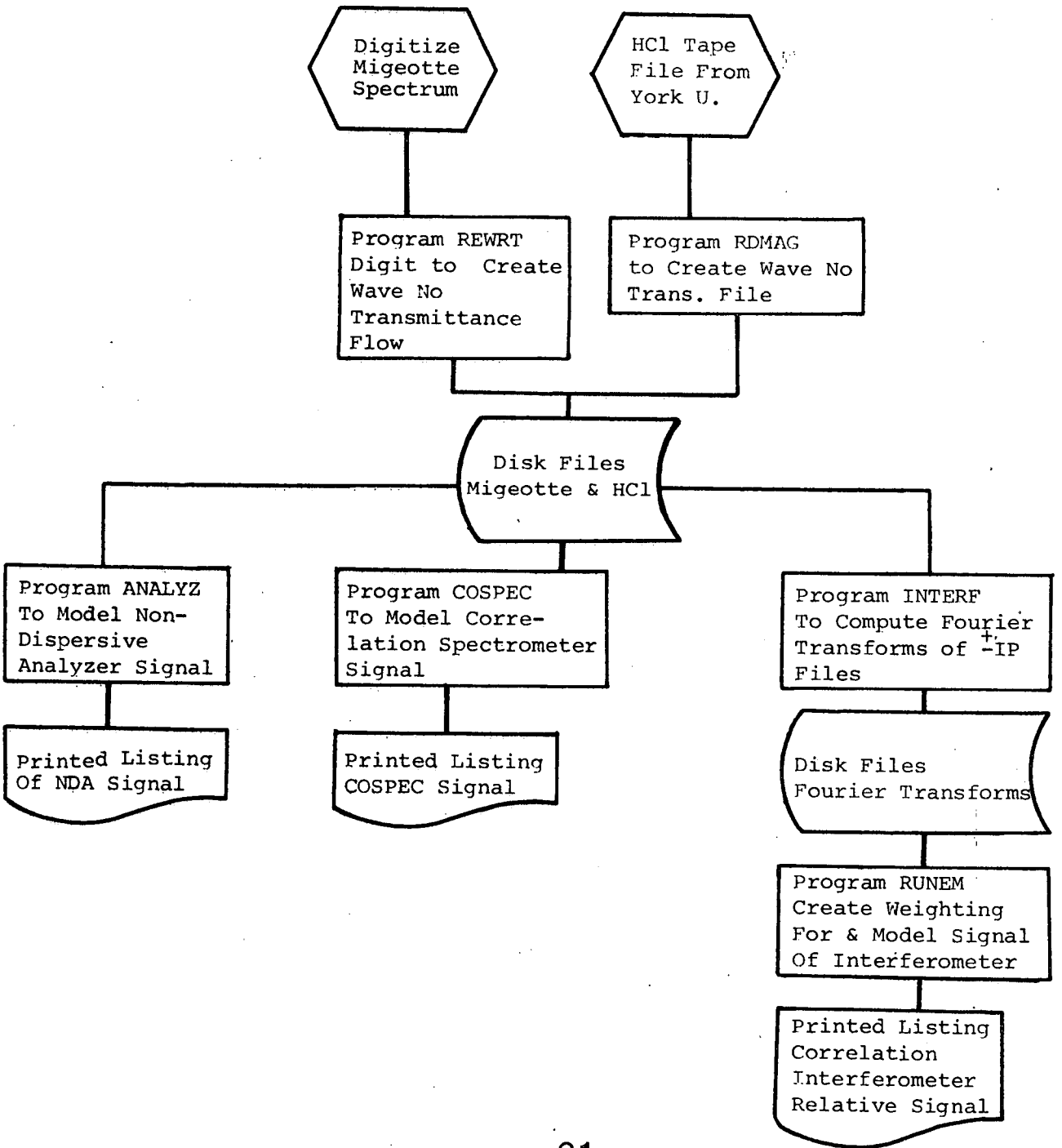

DATA FILES

(1) Atmospheric spectra profiles were obtained from The Solar Spectrum From 2.8 to 23.7μ Part 1, Photometric Atlas (Migeotte, Nevin, Swenson)

These profiles were digitized onto cards and placed onto disk files.

The disk files were run through programme RFWRT, which reversed the order of the data to allow conversion from wavelength to wavenumber; and programme DIGIT which eliminated digitizing errors by linearizing and rotating X-axis, splined Y-axis data to equal X axis intervals (.025 cm^{-1}) and output a disk fit of wavenumber versus transmittance.

Programme NORML normalized data to maximum Y = 1.0 and created a binary disk file across the wavenumber range of interest (2700 - 2910 cm^{-1}).

(2) A tape file of wavelength versus transmittance for HCl gas of various concentrations was obtained from a radiative transport computation done at York University. This tape file was run through programme RDMAG to convert the data from IBM to PDP equipment compatible mode, convert from wavelength to wavenumber, and spline to equal frequency intervals (.025 cm^{-1}). The new files were output onto disk over frequency range 2700 to 2910 cm^{-1}.

This procedure was repeated for each of three of the original tape files.

Instrument Modelling

(1) Non-dispersive Analyzer (NDA). Programme ANALY→ calculates the signal through the NDA due to HCl gas in the atmosphere by calculating the zero-gas correlating factor $C = \Sigma\left(M * IF * HCl_{cell}\right) / \Sigma(M*IF)$

where M is Migeotte solar spectrum transmittance.

IF is interference filter transmittance, and this was chosen to be the function

$(1-(F/Fo)^2)^3$ where F is frequency 1 $cm^{-1} \leq F \leq$ 200 cm and Fo = 100 cm^{-1}. This function approximates what may be expected for about a 90 cm^{-1} half width filter, and has a finite extent for ease in computing.

HCl cell is the HCl gas cell transmittance of a cell containing 0.1 atmospheres of HCl, and 1 cm length at 295°K.

The signal was computed as follows

$$\Sigma(M * IF * HCl_{atm} * HCl_{cell}) - C * \Sigma(M * IF * HCl^{i}_{atm})$$

Where HCl_{atm} is HCl gas in the atmosphere with concentrations of 1 ppm-m or 100 ppm-m. The programme also calculates the signal using the square root of the transmittance of Migeottes spectra as a measure of changes in signal due to different atmospheric amounts of interferent species.

(2) Correlation Spectrometer

The programme SPECT calculates signal resulting from correlation of two exit slit masks.

The programme sets up two sets of elements in the exit slit, MSK1 and MSK 2, at specified wavenumber locations which are on and off the HCl gas peak respectively.

The signal is then calculated for the gas and no-gas conditions as

$$S_{gas} = \left[\Sigma(M * HCl * IF).\ MSK1\right] - \left[\Sigma(M\ I\ HCl * IF).\ MSK\ 2\right]$$

which is resultant signal due to Migeotte solar spectrum (M), HCL atmospheric gas, and interference filter (IF) as before and

$$S_{no\ gas} = \left[\Sigma(M * IF).\ MSK\ 1\right] - \left[\Sigma(M * IF).\ MSK\ 2\right]$$

Is signal with no HCl gas present.

The output signal of COSPEC due to HCl gas alone is then

$$(S_{gas} - S_{no\ gas})$$

This output signal is calculated with 1 ppm-m and 100 ppm-m of HCl gas and also for a solar spectrum $\sqrt{M}$ (i.e. change in atmosphere). The mask elements are the triangular spectrometer response functions resulting from equal width entrance and exit slits (1.73 cm^{-1})

(3) Interferometer

The programme calculates the Fourier Transform of the input transmittance files, which yields both the amplitude and the phase of the interferogram output signal.

The programme applies the same interference filter over the input spectral range 2705 - 2905 cm^{-1} as used for the previous sensor calculations, $(1 - (F/Fo)^2)^3$.

This filtered data is then interpolated using the smoothing function

$$\left(\sin \frac{(2\pi\ f_c\ n)}{2\pi\ f_c\ n}\right) \left(\sin \frac{2\pi\ F_N\ n)}{2\pi\ F_N\ n}\right)^2$$

Where f_c is cut-off frequency

F_n is the apodizing frequency

n is an index of frequency location $1 \leq n \leq N$

This reduces the input data 1024 points. The fast Fourier Transform (FFT) is then applied to the 1024 points using the Cooley-Tuley algorithm, and files written into disk.

The FFT files are used by programme RUNEM to create a weighting function

which was used as the correlation function for the test interferograms.

The following library set of interferograms were computed:

$$S1 = \Sigma(\text{Migeotte} * \text{Interference filter})$$

$$S2 = \Sigma(M * IF * HCl\ (1\ ppm\text{-}m))$$

$$S3 = \Sigma(\sqrt{M} * IF * HCl\ (1\ ppm\text{-}m))$$

$$S4 = \Sigma(\sqrt[3]{M} * IF)$$

$$S5 = \Sigma(M * IF * HCl\ (100\ ppm\text{-}m))$$

$$S6 = \Sigma(\sqrt{M} * IF * HCl\ (100\ ppm\text{-}m))$$

A few samples of computed interferogram amplitudes are shown in Figure D1. The weighting function is created using the library interferograms S1, S3 and S4.

Table D1 shows the results of the application of the derived weighting functions to a range of interferogram segments. The uppermost number in each case is the deduced HCl burden deduced from S3 relative to S2 which had 1 ppm meter of HCl. The best interferogram segment should record 1.00 ppm-m. As seen from the table several regions allow a measurement of the expected burden (within a few percentage points). Furthermore the second and third numbers in each set is the computed burden for 100 ppm-m HCl burden. The number returned for a perfect measurement with a linear curve of growth would be 100 in every case. As can be seen the curve of growth is not quite linear. Further the third number is deduced for a different interferent spectrum from the second number. The table dramatically illustrates the interferent rejection capability of correlation interferometry analysis.

RELATIVE HCl MEASUREMENT OUTPUT

HCl RELATIVE S/N

Start / End Cm	1035	1045	1055	1065	1035	1045	1055	1065
.05	1.78 92.5 94.0				.455			
.06		1.16 92.3 92.3				.490		
.07	1.41 92.2 93.1		.766 91.7 92.0		.541 17.1		.293	
.08		.989 92.3 92.8		2.91 89.2 72.2		.529 16.7		.382
.09			.971 91.3 92.3				.374	
.10				1.04 91.1 92.3				.487 15.3
.165				1.03 90.6 91.2				.661 12.9
.375	1.10 90.0 90.6				1.08 11.9			

RUNEM MEASUREMENTS ON FFT'S S3, S5, S6, RESPECTIVELY FOR VARYING DELAY INTERVALS OF CORRELATION

(RELATIVE TO S2 = 1.0)

TABLE D1

Continued...

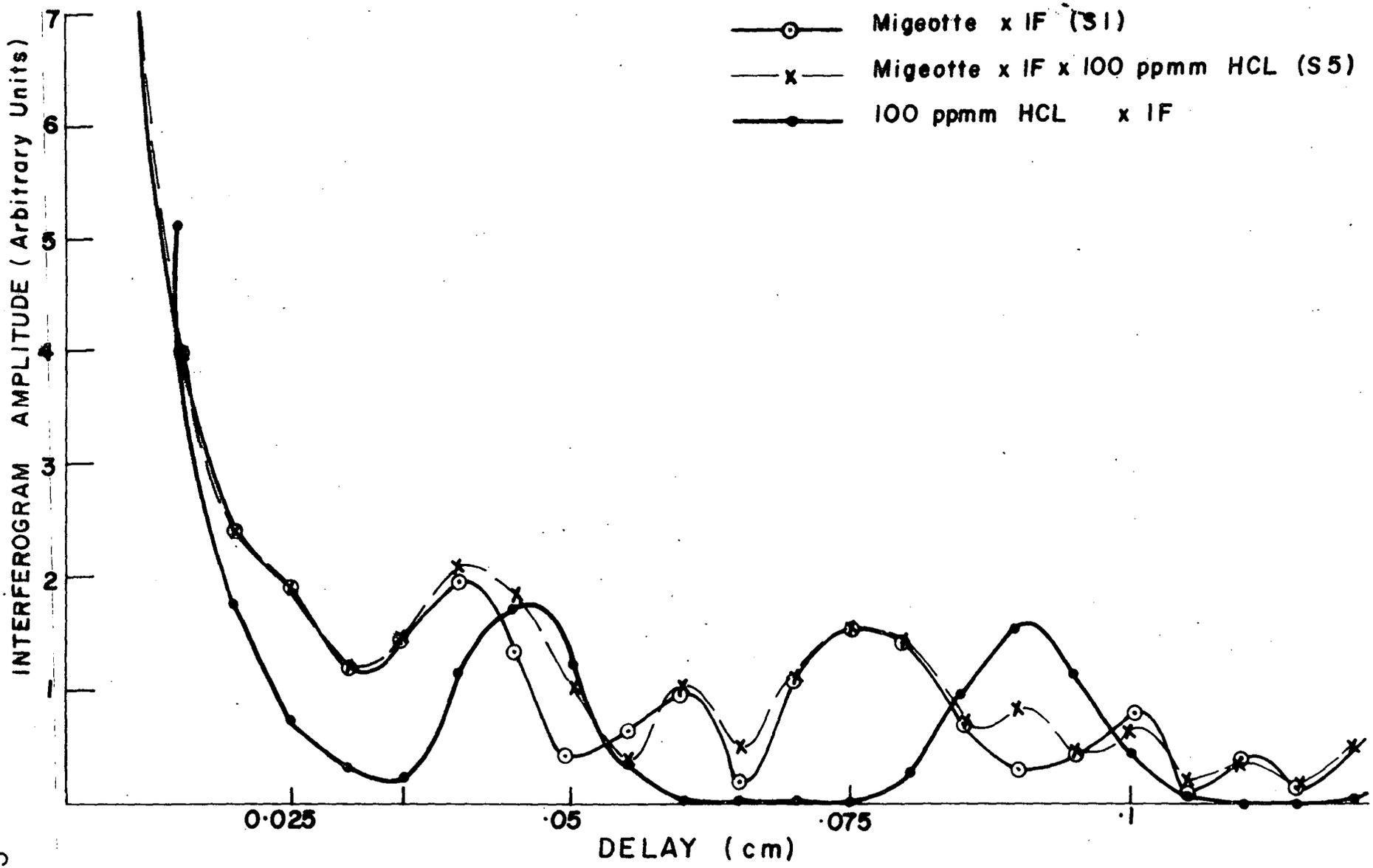

FIGURE DI. COMPUTED INTERFEROGRAM SEGMENTS